ORIGINAL ARTICLE

Evolution of a Miocene canyon and its carbonate fill in the pre-evaporitic eastern Mediterranean

J. Reolid[1] · O. M. Bialik[2] · Á. Puga-Bernabéu[1] · E. Zilberman[3] · J. Cardenal[4] · Y. Makovsky[5,6]

Abstract

Extensive canyons, excavated into the margins of the Levant Basin during the Oligocene–Miocene, are interesting case-studies for canyon fills in carbonate settings. The carbonate Pattish Formation, developed along the margins of the pre-evaporitic Messinian Beer Sheva Canyon in Israel, was investigated using both onshore seismic imaging and field data. The canyon has three main seismic facies of fill (1) Subparallel reflections mimicking the canyon´s morphology; (2) chaotic reflections overlying the subparallel ones, and (3) sigmoidal reflections, locally with sharp edges at the canyon margins. The first seismic facies corresponds to the pelagic marls of the Bet Eshel Formation. The other two seismic facies are, respectively, equivalent to bioclastic calcarenite clinobeds with slumps and channels, and to coral–stromatolite reefs and reef slopes of the Pattish Formation observed at outcrop. There were three phases of canyon development: (1) slope incision and headward erosion due to tectonic uplift and eustatic sea-level fall during the Early Oligocene, and large slope failure during the latest Middle Miocene; (2) platform incision and connection with a fluvial system in the Late Miocene related to falling sea level and tectonic uplift; and (3) canyon filling first by pelagic marls at the centre of the canyon, followed by calcarenite clinobeds at the canyon flanks formed by gravity flows. Finally, carbonate production at the margins of the canyon resulted in reefs and associated slopes prograding towards the canyon axis. The late canyon filling phase ended with the deposition of evaporites during the Messinian Salinity Crisis.

Keywords Messinian salinity crisis · Sediment gravity flows · Beer Sheva canyon · Carbonate slopes · Coral reefs

Introduction

Submarine canyons are major erosional features on the seafloor of most continental margins and they funnel sediment from the shelf to deeper-water settings to form submarine fans (Mutti and Normark 1987; Braga et al. 2001; Klaucke et al. 2004; Maier et al. 2020). In submarine canyons, sediment gravity flows generated by storms, direct discharge of river-born sediment or sediment supplied by longshore currents into canyon heads, and those that may evolve through flow transformation from slumps (e.g., canyon flank failures), are the most frequent transport mechanisms down-canyon (Puig et al. 2004; Talling 2014; Gamberi et al. 2015; Gamberi 2020).

✉ J. Reolid
jreolid@ugr.es

✉ O. M. Bialik
obialik@campus.haifa.ac.il

1 Departamento de Estratigrafía y Paleontología, Universidad de Granada. Avenida de la Fuente Nueva SN, 18071 Granada, Spain

2 Marine Geology and Seafloor Surveying, Department of Geosciences, University of Malta, Msida MSD 2080, Malta

3 Geological Survey of Israel, 30 Malkhe Israel Street, 95501 Jerusalem, Israel

4 Departamento de Ingeniería Cartográfica, Centro de Estudios Avanzados en Ciencias de la Tierra, Energía y Medioambiente (CEACTEMA), Geodésica y Fotogrametría, Universidad de Jaén, Campus Las Lagunillas sn, 23071 Jaén, Spain

5 The Dr. Moses Strauss Department of Marine Geosciences, Charney School of Marine Sciences, University of Haifa, Mount Carmel, 3498838 Haifa, Israel

6 Hatter Department of Marine Technologies, Charney School of Marine Sciences, University of Haifa, Mount Carmel, 3498838 Haifa, Israel

Submarine canyons in modern carbonate and mixed carbonate–siliciclastic settings are common features in a wide range of water depths (up to > 5000 m) (Exon et al. 2005; Mitchell et al. 2007; Puga-Bernabéu et al. 2011, 2013; Tournadour et al. 2017; Mulder et al. 2019). However, in the ancient record only their shallowest parts (i.e., canyon head), which are commonly excavated into a carbonate platform, are in general preserved (Buchbinder et al. 1993; Buchbinder and Zilberman 1997; Braga et al. 2001; Puga-Bernabéu et al. 2008). Filling geometries depend on the stage of canyon evolution (erosion, bypass, deposition and filling), the sedimentary processes acting in the canyons, and the nature of the sediment delivered to the canyons. In carbonate settings, carbonate production at the canyon head and margins (e.g., reef barriers) can largely influence the sedimentary fill (Puga-Bernabéu et al. 2011, 2013, 2014).

The Beer Sheva Canyon (SE margin of the Levant Basin, Israel) is an example of a submarine canyon, where the sedimentary fill is determined not only by sediment reworking and supply from the adjacent factory area, but also controlled by changes in carbonate production inside the canyon (i.e., fringing reefs attached to the canyon flanks). The Middle–Upper Miocene fill of the Beer Sheva Canyon consists of a thick carbonate succession including a variety of facies, from pelagic marls to shallow-water carbonates ranging from calcarenites to fringing reefs (Buchbinder et al. 1993; Buchbinder and Zilberman 1997). The coral reefs are present at the top of the canyon fill succession and predate the Messinian Salinity Crisis (MSC) (Buchbinder and Zilberman 1997). Such an age is useful in the regional context of the Mediterranean Sea. Most of the available studies on the Mediterranean Miocene reefs and associated carbonate slopes predating the MSC are focussed on western Mediterranean outcrops (Dabrio and Esteban 1981; Pomar 1991; Braga and Martín 1996; Reolid et al. 2014, 2017a,b; among many others), while information from the eastern Mediterranean is relatively scant (Buchbinder et al. 1993; Buchbinder 1996; Buchbinder and Zilberman 1997; Papadimitriou et al. 2018; Coletti et al. 2019).

The main objective of this study is to understand the tectono-eustatic evolution of the Beer Sheva Canyon in Israel based on the analysis of the facies and geometries of its carbonate fill. The factors controlling the filling geometries and facies composition and their distribution are discussed, along with interpretations as to how they evolved in relation to tectonic and sea-level changes occurring in the eastern margins of the Mediterranean prior to the MSC. These results go far beyond the current understanding of the regional sedimentology and may have an impact for carbonate sedimentological models in general and of ancient shelf-incising canyons, in particular.

Geological setting

The Neogene of the Mediterranean was a period of fundamental changes, the loss of connectivity to the Indian Ocean in the Early to Middle Miocene (Bialik et al. 2019, Cornacchia et al. 2021) and with the Atlantic in the Late Miocene (Martín et al. 2001, 2009, 2010; Betzler et al. 2006; Braga et al. 2010; Tulbure et al. 2017; Capella et al. 2018). These changes were most dramatic in the eastern Mediterranean and notably in its easternmost basin—the Levant Basin. The Levant Basin formed during the Late Palaeozoic and earliest Mesozoic. The margins of the Levant basins developed above an inherited geometry of a Cretaceous carbonate platform (Steinberg et al. 2008; Gardosh et al. 2011). During the Late Eocene to Early Oligocene, the Levant margin was a passive one and a morphological escarpment had developed between the deep Levant Basin and the inland range (Bar et al. 2013). By the Miocene, the margin configuration was similar to the present one, albeit with a smaller shelf extending into the present coastal plain. The formation of a 1500–2000 m high escarpment favoured the incision of deep submarine canyons, including the Afiq canyon, that was the offshore continuation to the west of the long stream named "the Beer Sheva Canyon" (Neev 1960), the subject of this study (Fig. 1). The evolution of these canyons occurred during a period of sustained uplift of the region, driven by both the far-field Afar Dome, the opening of the Red Sea and the compression related to the Arabia/Eurasia collision (Avni et al. 2012; Bar et al. 2016). The Beer Sheva Canyon is a Late Oligocene to Early Miocene canyon that is represented today by a 270 m deep valley buried under the city of Beer Sheva (Israel) (Neev 1960). Most of the canyon is filled with Late Miocene marine chalk and marl of the Bet Eshel Formation (Gvirtzman and Buchbinder 1969). The filling sequence is capped by a 30–40-m-thick shallow-marine limestone of the Late Miocene Pattish Formation (Buchbinder et al. 1993; Buchbinder and Zilberman 1997; Fig. 2). An erosion surface separates the Pattish Formation from the overlying 20–30-m thick, Pliocene, shallow-marine, sandy to calcareous Pleshet Formation. This surface, probably related to the drawdown during the Messinian Salinity Crisis (Buchbinder and Zilberman 1997), truncated most of the calcareous cover of the Pattish Formation from the Beer Sheva Canyon, apart from several relics scattered along its margins. As a result of differential uplift, the erosion surface presently extends from outcrops in the east to the subsurface in the west. To the west, within the Afiq canyon, an Oligocene to Messinian sequence was deposited and filled in and buried by the Pliocene Nilotic sediments of the Yafo Formation (Druckman et al. 1995).
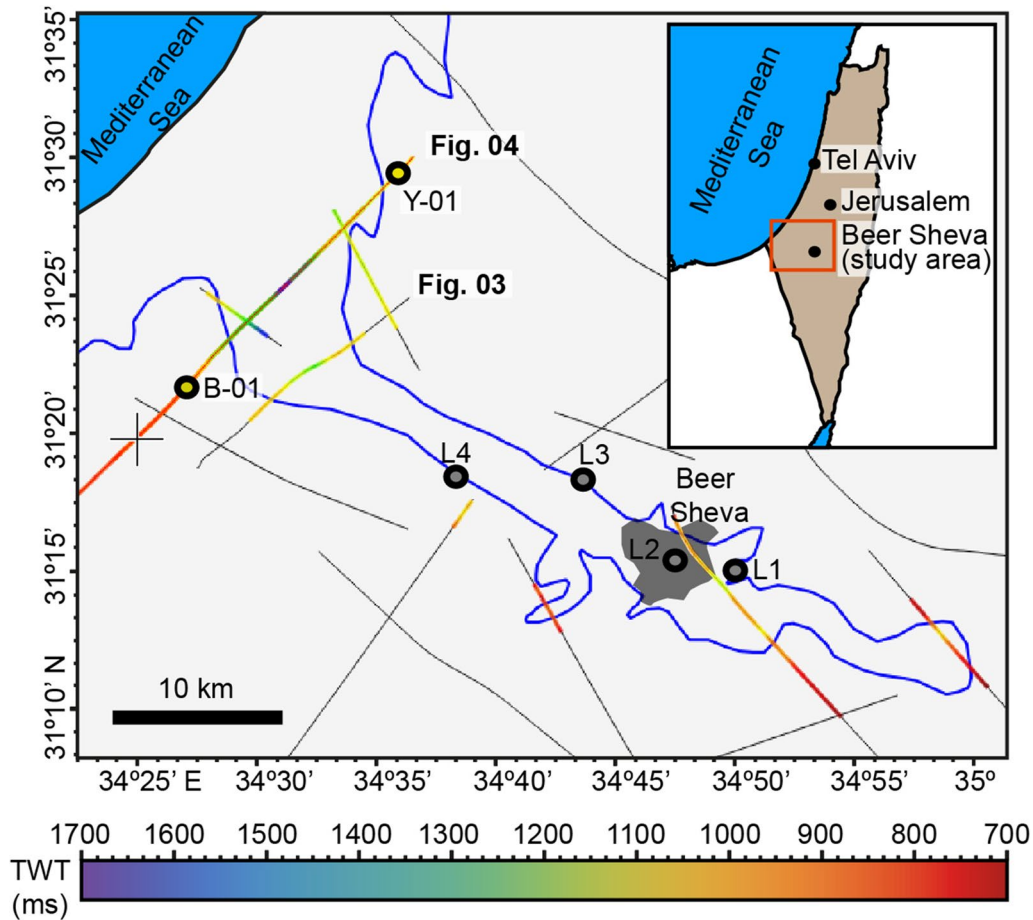
Fig. 1 Location of the Late Miocene Beer Sheva Canyon in Israel, eastern Mediterranean. The blue line outlines the morphology of the canyon according to Buchbinder and Zilberman (1997). Thin black lines are the available seismic profiles. The thickness of the canyon fill in TWT (ms) is shown in selected profiles. The grey dots represent the study locations (L1—Hativat HaNegev Interchange, L2—Beer Sheva Quarry, L3—Nahal Olim, L4—Ofakim Park). Yellow dots represent the studied boreholes (B-01 Bessor-01, Y-01 Yakhin-01). Grey shaded the contour of the city of Beer Sheva
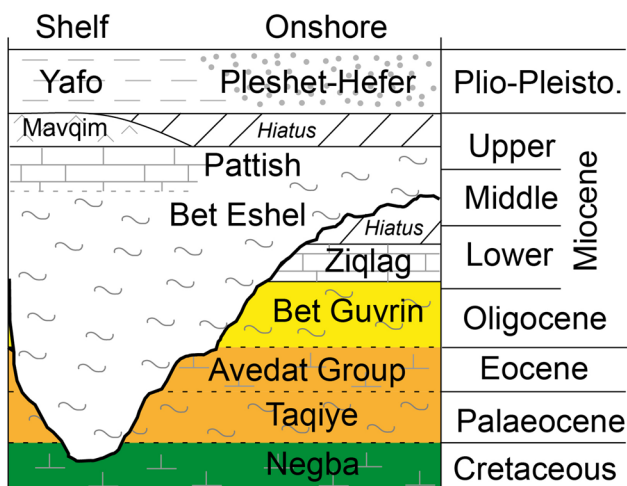

Fig. 2 Stratigraphy of the area of Beer Sheva, including the Pattish Formation which corresponds to the shallower materials of the Beer Sheva Canyon fill, subject of this study

Materials and methods

The study subject, the Beer Sheva Canyon and its fill, the materials of the Bet Eshel Formation and Pattish Formation (Fig. 1) were first investigated through fieldwork that included: (1) the definition of the sedimentary facies based on field properties and supported by the petrographic study of 30 thin-sections from representative samples; and (2) the acquisition of high-resolution photographs that were integrated into a three-dimensional (3D) photogrammetric model that allowed the measurement of clinoform dimensions and orientation at the walls of the Beer Sheva Quarry.

The terrestrial photogrammetric survey was planned to model the Beer Sheva Quarry (Location 2; Fig. 1), the best exposed outcrop of the Pattish Formation in the area. The camera was a SONY DSC-RX100M4 with a Zeiss 8.8–25.7-mm zoom lens. Only the wide-angle end position (8.8 mm) was used to avoid errors due to the instability of

zoom lenses. This compact camera has a resolution of 20 MP (5472×3648) and a pixel size of 2.4 μm. Handheld photographs, under good daylight conditions, were taken at two different distances. First, a general network with almost parallel shots covered the Southern and Western sectors of the outcrop at distances between 30 and 40 m. Additional parallel and convergent images were taken at closer distances between 5 and 15 m to cover the outcrop in detail (see image in Table 1). A total of 588 images was used to build the 3D model.

Images were processed with the photogrammetric software Agisoft Metashape Pro 1.5.2 (Agisoft 2021). Since any external ground control points (GCP) were surveyed (for example with GNSS techniques), the image block was first adjusted only in scale with the control distances measured at the outcrop using targets (printed black circles and crosses on white background) and a laser distance meter (TECCPO[R]). The final adjustment error was 1.9 pixels and the root mean square error (RMS) of the control distances was ± 0.063 m (Table 1). Finally, by measuring some identifiable points in Google Earth, the arbitrary reference system was approximately translated and rotated to a regional coordinate system for Israel (ETRS89 UTM 36N; EPSG: 3048).

After the block adjustment was considered optimal, a 3D point cloud densification process was launched with Agisoft Metashape. Once the dense point cloud was edited, a mesh (with photorealistic textures) was generated and the final 3D model of the outcrop was obtained. The final dense point cloud consisted of 24,946,751 3D points and the surveyed area covered 3312 m^2, which implies a point density of 0.9 points/cm. The final mesh, once edited and decimated to reduce redundant information, had 4,792,554 faces (triangles). CloudCompare V2 (CloudCompare 2021) was used for further data processing, as well as for tracing bedding surfaces and measuring their orientation, e.g., canyon flank bedding of successive clinoform units in this study.

The stratigraphic architecture was complemented with the study of seismic profiles from the area of Beer Sheva to fill the gaps between the dispersed Upper Miocene outcrops. The analysis combined a set of 13 time-migrated seismic sections of different vintages (Table 2), which were selected based on the adequacy of their imaging quality from the State of Israel Ministry of Energy data archive. Seismic analysis was carried out at the Applied Marine Exploration Laboratory, University of Haifa, using Paradigm, Emerson's Exploration & Production software, for visualization of the seismic profiles. Representative seismic horizons, including the base of the Beer Sheva Canyon and the contacts among the successive stratigraphic units, were traced and tied with stratigraphic markers in the wells Bessor-01 and Yakhin-01 (Fig. 1). The general outline of the Beer Sheva Canyon and the age model for its fill deposits were derived from the drillhole reports (Martinotti et al. 1981; Fleischer and Varshavsky 2002) and mapping presented by Buchbinder et al. (1993), Buchbinder and Zilberman (1997), and Zilberman (2018).

Results

Seismic data description

The lowermost reflections in the seismic profiles have moderate to high amplitudes and, according to Fleischer and Varshavsky (2002) well formation tops, correspond to the top part of the Negba Formation (Figs. 3, 4). Overall, the reflections are laterally continuous, especially in the intervals with the higher amplitude. The Negba Formation is overlain by the Taqiye Formation and the chalks and marls

Table 1 Main data of the photogrammetric survey at Beer Sheva Quarry: camera data, photogrammetric network (a ground plan of network geometry is included) and 3D model

Camera	SONY DSC-RX100M4
Lens focal length	8.8 mm
Image resolution (pix)	5472 x 3648
No of images	588
Mean GSD	2.92 mm
Reprojection error	1.92 pix
No. of 3D points	24946751
Outcrop coverage area	3213 m^2
3D point density	0.9 points/cm
Mesh (No. of faces)	4792554
RMS Control distances	±0.063 m
Split test check	-0.036 m ±0.025 m

Table 2 Basic parameters of the seismic lines shown in Fig. 1

Profile	CMP Interval [m]	Nominal Fold	Sampling interval [msec]
DS0316	25	120	4
DS0513	30	120	4
DS0543	30	120	4
DS1064	30	120	4
DS3092	20	120	4
DS3561	27,5	120	4
DS3576	25	120	4
EM3503	27,5	120	4
EM3510	27,5	120	4
EM3690	25	120	4
EM7736	25	120	4
EM7754	25	120	4
EM7763	25	120	4
GI3558	25	120	4
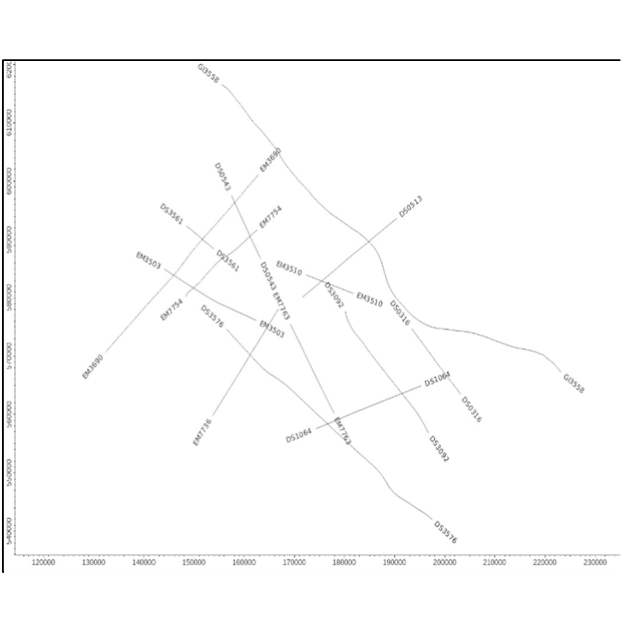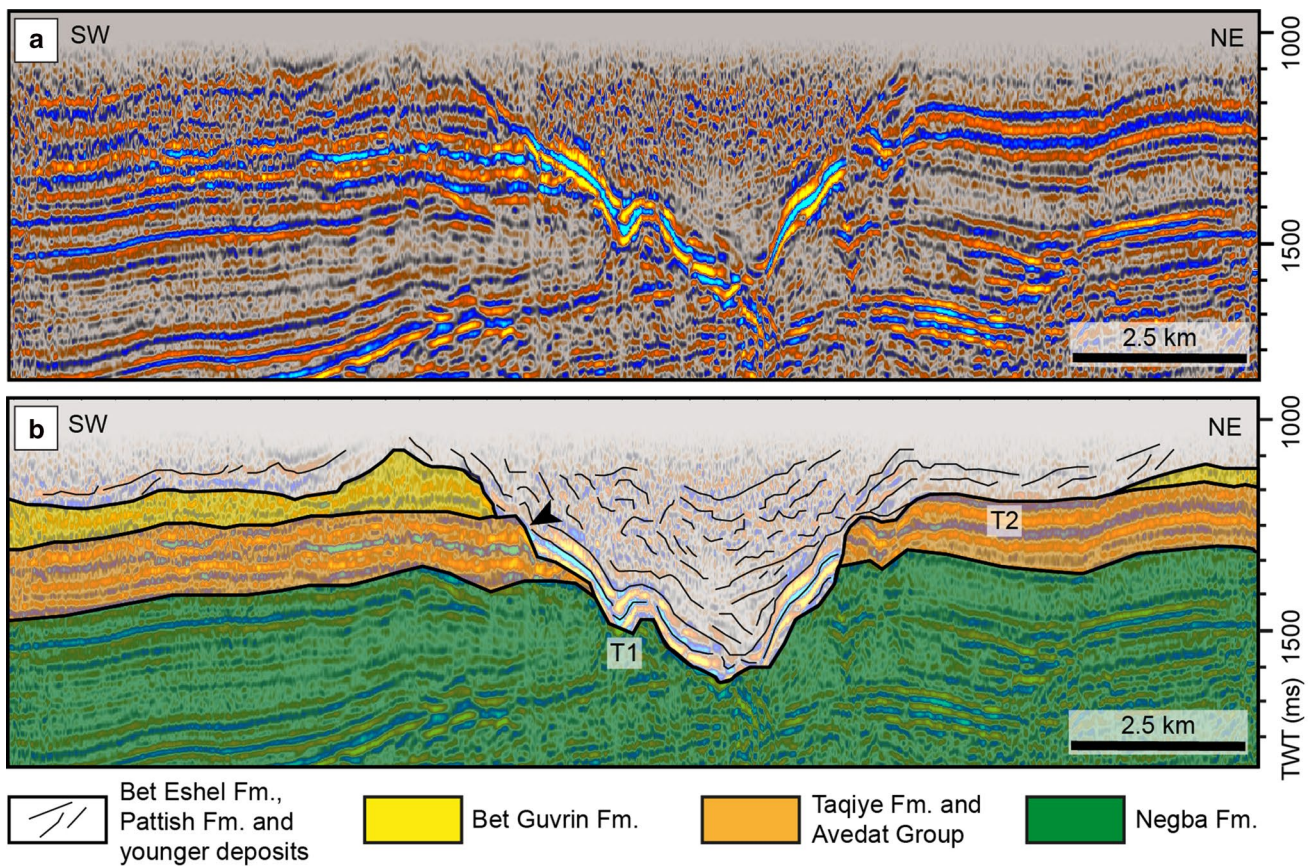
Fig. 3 SW–NE overview of the Beer Sheva Canyon at its northern part (see Fig. 1). **a** Seismic profile and **b** interpretation with the boundaries of the main formations. Note that the canyon fill unconformably overlies the excavated Cretaceous basement of the Negba Formation, forming a first terrace (T1), and overlying Taqiye Formation and Avedat Group, forming a second terrace (T2, black arrow), and thin Oligocene Bet Guvrin Formation
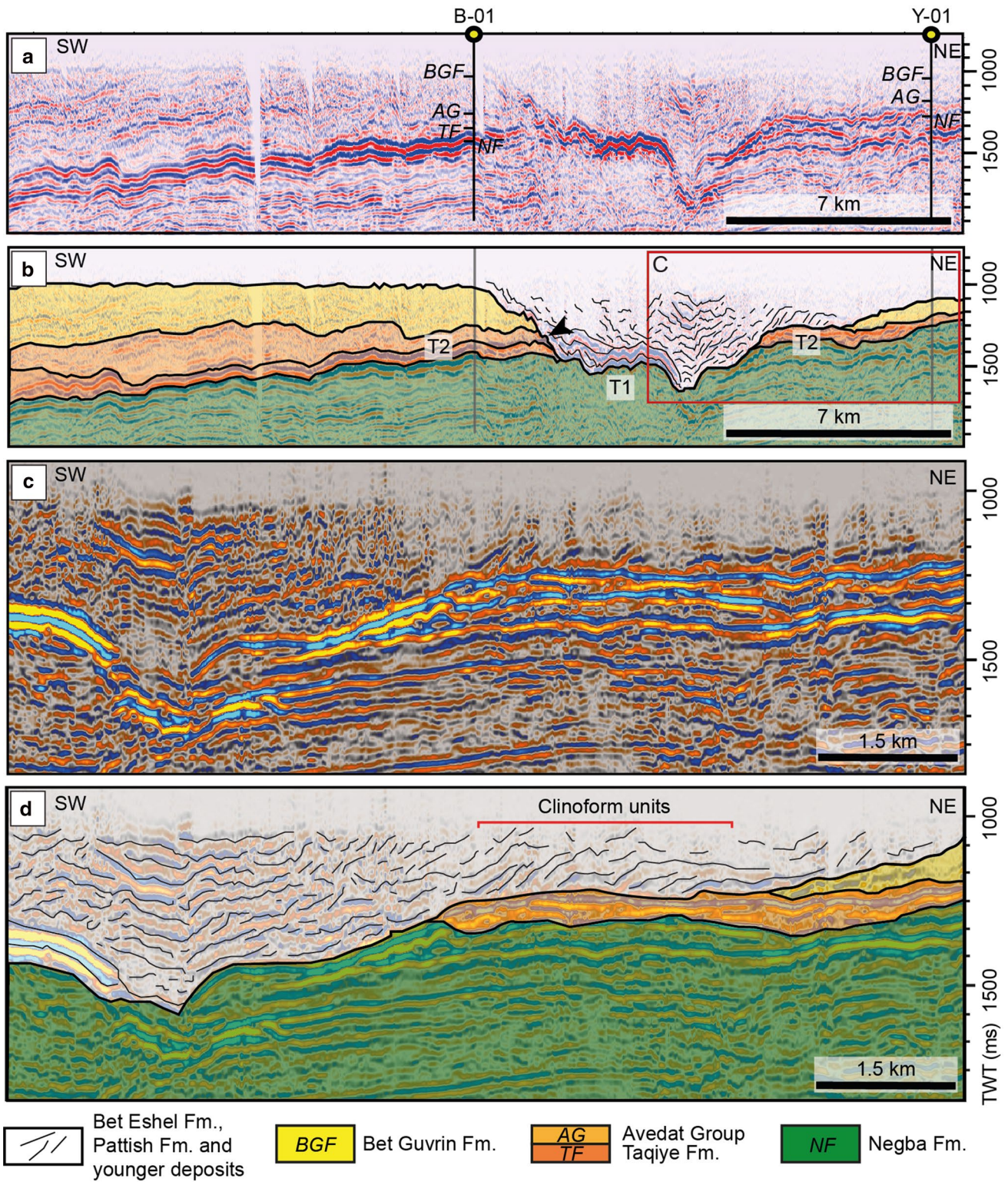
Fig. 4 SW–NE overview of the Beer Sheva Canyon at its northernmost part (see Fig. 1). **a** Seismic profile with location of the oil and gas wells, and **b** interpretation with the boundaries of the main formations (black arrow indicates the steepest flank erosion corresponding to the Taqiye Formation and Avedat Group at the southern canyon flank). T1—first terrace, T2—second terrace. **c** Close-up of the channel fill and **d** interpretation. Note the southward prograding clinoforms of the Pattish Formation at the canyon's margins

of the Eocene Avedat Group (Adulam and Maresha Formations), which cannot usually be differentiated in the seismic profiles (Fig. 3). When visible, the Taqiye Formation interval consists of a thin package (150 ms) of very high amplitude reflections with high lateral continuity (Fig. 4). The overlying Avedat Group is marked by parallel to chaotic reflections of low amplitude (Fig. 4) and is followed by the Bet Guvrin Formation that is marked by moderate amplitude and parallel to subparallel reflections and represents the top of the sequence (Figs. 3, 4).

All these formations are partially eroded by the Beer Sheva Canyon as shown by their truncated reflections in correspondence to the canyon incision (Figs. 3, 4). The latter extends laterally for up to 10 km in cross section (Fig. 3) and reaches > 17.5 km close to its mouth in the Mediterranean Sea (Figs. 1, 4). The depth of the canyon incision increases from east to west with roughly 900 ms in TWT in the easternmost part of the canyon, to around 1100 ms near study locations 1 and 2 (Fig. 1). The canyon depocenter in its deepest part, close to its mouth, is 1700 ms in TWT (Figs. 1, 4). Two terraces are recorded at the top of the Negba Formation and the top of the Avedat Group (Figs. 3, 4). The canyon fill comprises the deposits of the Bet Eshel Formation, the Pattish Formation, and younger materials. They consist of low to moderate amplitude reflections which mimic the morphology of the base of the canyon in its central part and become chaotic towards the steep canyon flanks (Figs. 3, 4). Sigmoidal reflectors prograding towards the canyon axis are also observed in the Pattish Formation (Fig. 4d).

Outcrop data description

The study of the Pattish Formation was carried out at four locations corresponding to the canyon flanks and close the canyon axis of the Beer Sheva Canyon (Fig. 1).

Location 1—Hativat HaNegev Interchange

This section is a 30 m long road cut with an excellent outcrop exposure (31°15′36.6″N, 34°49′50.0″E). The sedimentary succession begins with a few m-thick Eocene chalk (likely from the Avedat Group), into which the Beer Sheva Canyon was excavated (Fig. 5a, b). The surface separating the Avedat Group from the canyon fill is irregular and has low relief (Fig. 5c, d). The basal part of the canyon fill consists of a clast-supported, pebble-to-cobble-size breccia of chalk clasts around 4-m thick, which locally intercalates with bioclastic sand lenses (Fig. 5c, d). Overlying the basal breccia, the canyon fill includes coarse-grained bioclastic sands with a local mixture of siliciclastic grains, mostly sand-sized quartz and feldspar. The recognizable bioclasts are mostly gastropods and bivalves, but most of the grains consist of unidentifiable sand-sized bioclastic fragments. The sediment is intensely bioturbated and bedding surfaces are only locally preserved. When preserved, beds are up to 15 cm thick and display the same inclination of the canyon flank (Fig. 5e). Some of these beds even display small-scale soft-sediment deformation in their lower part (slumps, Fig. 5f). In contrast, some of the beds display evidence of early lithification highlighted by borings of *Lithophaga* sp. (Fig. 5g, h).

Location 2—Beer Sheva Quarry

This section is located in the historical Ottoman Beer Sheva Quarry in the centre of the city of Beer Sheva (31°15′41.8″N, 34°47′20.3″E). With 10 m of exposed thickness and an area of 44,000 m², it is the most extensive outcrop in the area. The bulk of the outcrop consists of a succession of clinoforms dipping southward between N160E and N244E. The average dip direction of the clinoforms, N212E obtained from the photogrammetric model, is roughly perpendicular to the orientation of the canyon axis according to the canyon tracing by Buchbinder and Zilberman (1997) (Figs. 1, 6a, b). This is consistent with the depocenter, canyon axis, traced in the seismic line to the east of Location 2 (Fig. 1). Locally, boulders of chalk derived from the Eocene succession below the erosional surface are interbedded within the carbonates.

The sedimentary succession comprises three parts according to their main facies and beddings types: (1) gently inclined clinoforms with well-bedded bioclastic calcarenites and calcisiltites, (2) channelized calcarenites to calcirudites, and (3) nodular calcarenites (Figs. 6, 7). The gently inclined clinoforms are comprised of well-bedded bioclastic calcarenites with variable grain-size and sorting, with the dominance of moderately sorted beds of fine to medium sand, making up the majority of the studied section. As a general trend, in each clinoform the sediment grain-size decreases from coarse-grained calcarenites in the proximal part of the clinoform beds to fine-grained calcarenites at their distal ends. The clinoform units dip up to 21° (mean ~ 15°) SSE towards the canyon axis (Fig. 6c, d). The clinoforms on average are up to 9 m high and 33 m wide. The thickness of individual clinoform units varies between 40 and 100 cm with internal bedding ranging in thickness between 5 and 20 cm. The top of these beds is intensely bioturbated, especially at the distal part of the clinobeds. Towards the canyon axis, the clinoforms units change into calcisiltites, which are mostly confined to the distal part of the clinoforms.

The uppermost part of the clinoforms is locally truncated by large channels, up to 10 m wide and 4 m deep (Fig. 7a, b). The axes of these channels are oriented towards the southeast, (between N122E and N129E), being approximately parallel to the direction of the Beer Sheva Canyon (Fig. 1). The erosional bases of the channels truncate the finer-grained clinoforms (Fig. 7c). Beds crudely parallel the outlines of the channels and gradually fill them. The channel
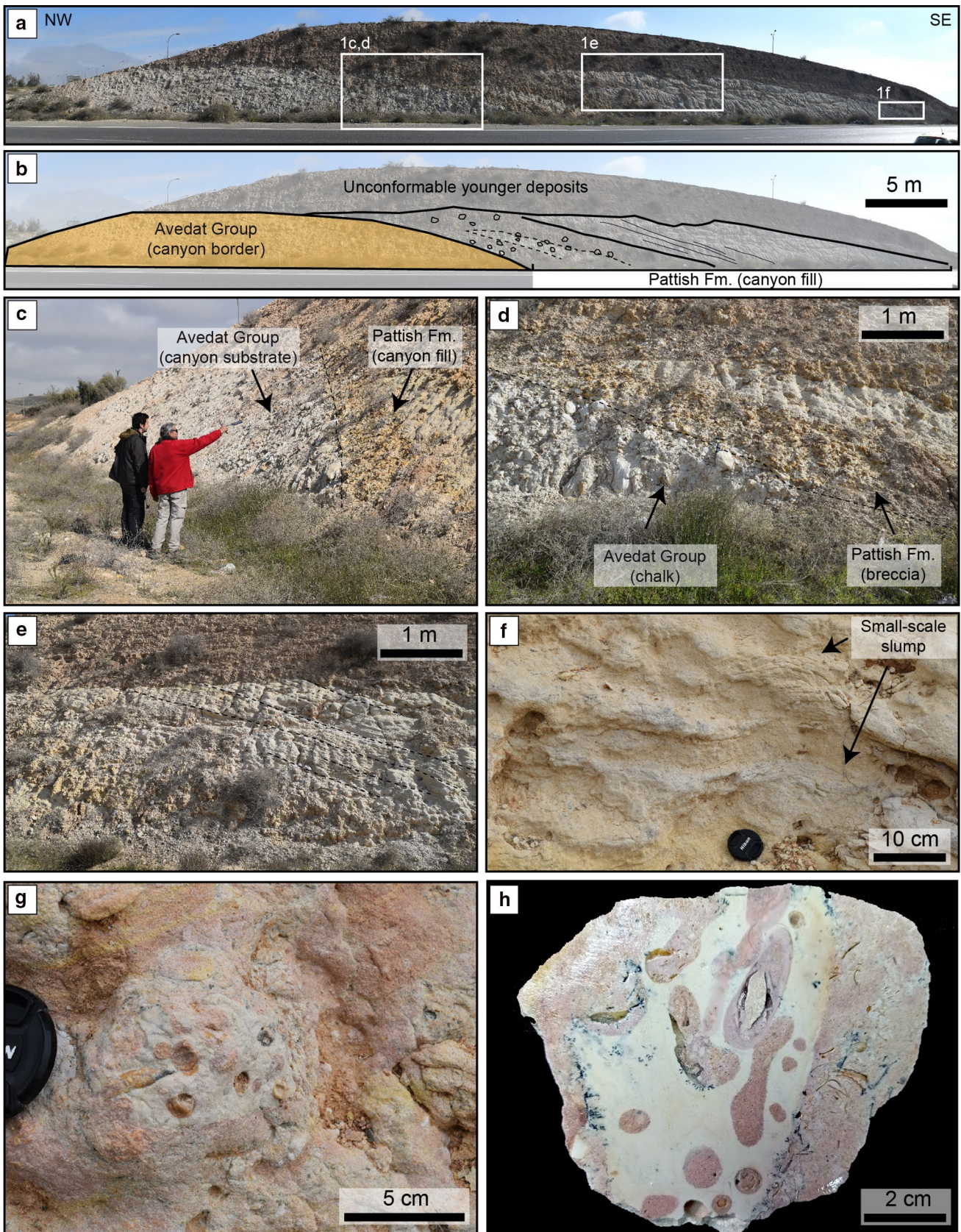
◄**Fig. 5** Location 1—Hativat HaNegev Interchange. **a** Overview of the outcrop and **b** interpretation of the excavated deposits and the canyon fill over the underlying substrate. **c, d** Close-up of the breccia that separates the Eocene deposits from the canyon fill. **e** Bedding surfaces inclined following the morphology of the channel. **f** Example of small-scale slumps in the clinobeds. **g, h** Field photograph and polished slab of *Lithophaga* sp., indicative of early lithification of the clinobeds

fill is characterised by a breccia bearing cm-scale lithoclasts and boulders (up to 60 cm in diameter) made up of bioclastic limestone that changes upward into a massive calcirudite and in turn to a poorly laminated calcarenite with abundant trace fossils. The majority of the bioclasts in these beds are mollusc fragments, but some coral debris is locally present (Fig. 7d).

Above the clinoforms and the channels, the top of the succession is dominated by nodular calcarenites with abundant vertical trace fossils (mostly *Thalassinoides*). This facies has subhorizontal bedding and unconformably overlies the bioclastic calcarenite clinoform beds (Fig. 6).

Location 3—Beer Sheva´s countryside

The outcrop is limited to a few exposed beds and the wall of a trench (31°18′24.3″N, 34°43′43.4″E). These deposits were mapped as part of the Late Miocene fill of the canyon (Zilberman 2018). Their exact stratigraphic position is unclear, but they are presumably lateral equivalents to carbonate deposits in Location 2. The facies consists of relatively well-sorted medium-to-fine-grained cross-bedded calcarenites (Fig. 8a). The components are abundant debris of coralline algae, bryozoans and molluscs. The beds are around 40 cm thick and have coarser grain-size basal units. Bioturbation, commonly consisting of vertical burrows, is locally intense and alternates with the cross-laminated beds.

Location 4—Ofakim Park

This site (31°18′22.7″N, 34°38′11.5″E) is located on the south margin of the Beer Sheva Canyon according to the outline of the canyon by Buchbinder and Zilberman (1997) (Fig. 1). Here, two facies are observed: (1) gently inclined calcirudite–calcarenite clinoform beds with abundant rhodoliths; (2) reef framework facies. Because of the vegetation, the stratigraphic relationship between these two facies is not precise, but the reef facies apparently overlies the rhodolith beds.

The gently inclined clinoforms consist of an alternation of bioclastic calcarenites and calcirudites made up of coralline red algal fragments and mm nodules, bryozoan and mollusc remains intercalated with rhodolith-rich beds (Fig. 8b). The rhodoliths range in size between 3 and 5 cm and locally form pavement beds. The rhodoliths are usually floating in a poorly sorted medium-grained bioclastic sand.

The reef framework facies displays diverse coral species including *Tarbellastrea* and *Porites*, the latter being the most abundant (Fig. 9). This facies occurs as an accumulation of framework blocks, but some of the framework preserves its original orientation according to the occurrence of *Porites* skeletons in life position. *Porites* skeletons are covered by thin coralline algal–foraminiferal crusts overgrown by thick stromatolitic crusts, usually preserved as massive micritic masses, where some macroinvertebrates are preserved. A bioclastic matrix fills in the remaining spaces between the *Porites* tubes. According to the stratigraphy of Buchbinder et al. (1993), this facies is the latest fill of the Pattish Formation and is overlain by the evaporites of the MSC.

Seismic to outcrop correlation

The outcrops of the sedimentary canyon fill in the Beer Sheva area are Late Miocene to Early Pliocene (Martinotti et al. 1981; Zilberman and Buchbinder 1997). Oligocene fill is exposed to the north of the study area near Kiryat Gat, where the substrate into which the canyon was excavated in the Eocene Avedat group (Hirsch 2005) is seen at Location 1. The presence of well-developed clinoforms at Location 2 of the same age (Zilberman 2018) as the recovered material in the wells at the mouth of the Beer Sheva Canyon to the west in the subsurface (Martinotti et al. 1981; Fleischer and Varshavsky 2002), is a small-scale equivalent of the clinoform units observed in the seismic profiles (Fig. 4d). This would suggest that the deposits from the Beer Sheva Quarry are the marginal canyon fill situated on higher terraces on the canyon, and that the marl and deeper deposits of the canyon axis are likely located towards the south of the city (Fig. 1). The reefs of Location 4 probably also occurred on a higher terrace that in the present day is not recorded in the area of Beer Sheva to the east and that is below the surface in the westernmost part of the canyon (Figs. 1, 4). The different absolute elevation of these terraces in the east and west is ascribed to the differential uplift of the region with the eastern side uplifting and western subsiding (Buchbinder et al. 1993; Bar et al. 2016).

Discussion

Sedimentary model of canyon filling processes

The sedimentary fill of the Beer Sheva Canyon comprises facies indicative of different sedimentary processes, mainly divided into: (1) products of the erosion and incision of the
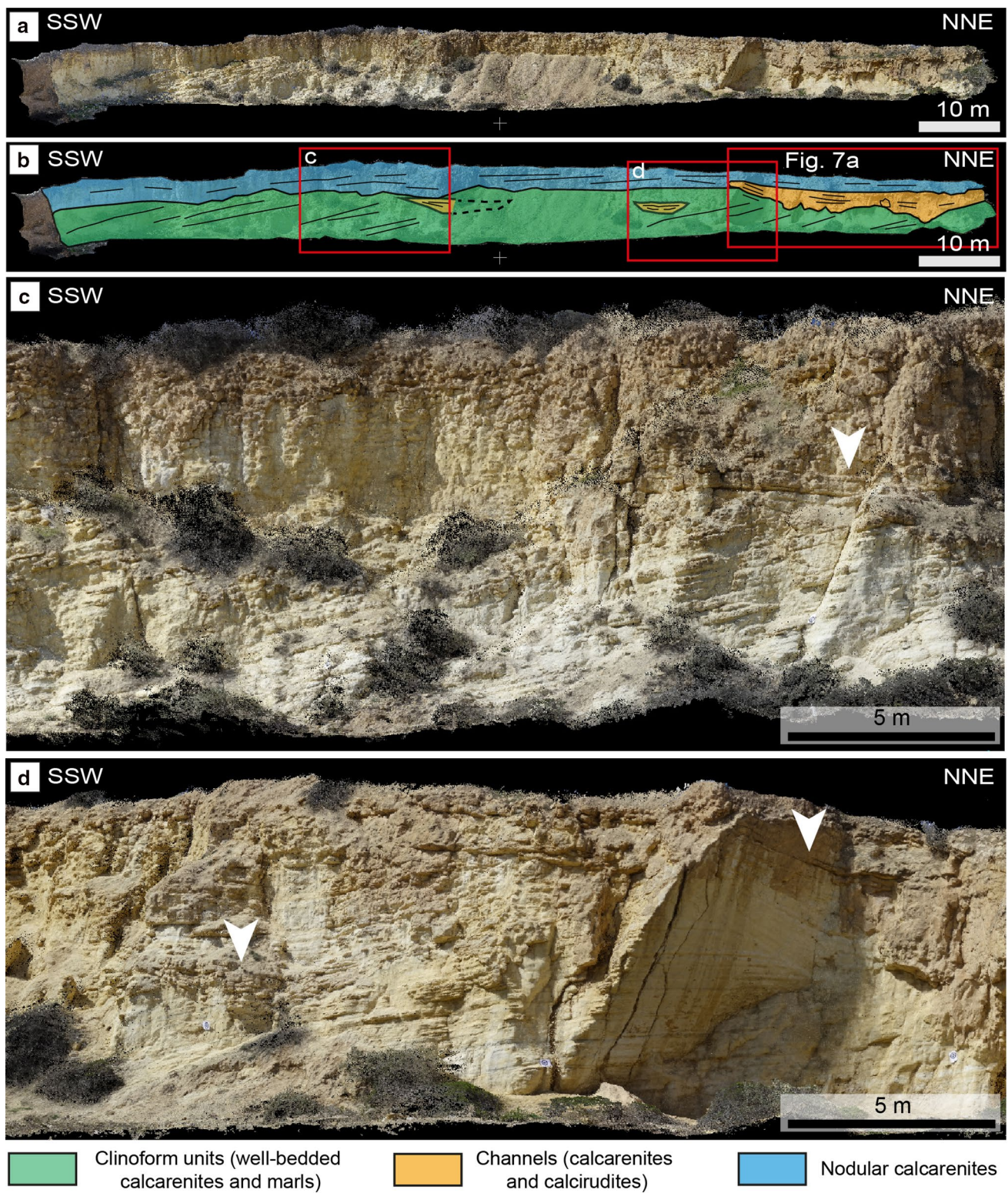
Clinoform units (well-bedded calcarenites and marls)

Channels (calcarenites and calcirudites)

Nodular calcarenites

Fig. 6 Location 2—Beer Sheva Quarry. **a** Overview of the photogrammetric model of the outcrop and **b** interpretation of the different canyon fills. **c, d** Close-up view of the wall of the quarry with observable clinoform units that change upward into subparallel beds of nodular calcarenites. White arrows mark channels parallel to the canyon axis that truncate the clinobeds
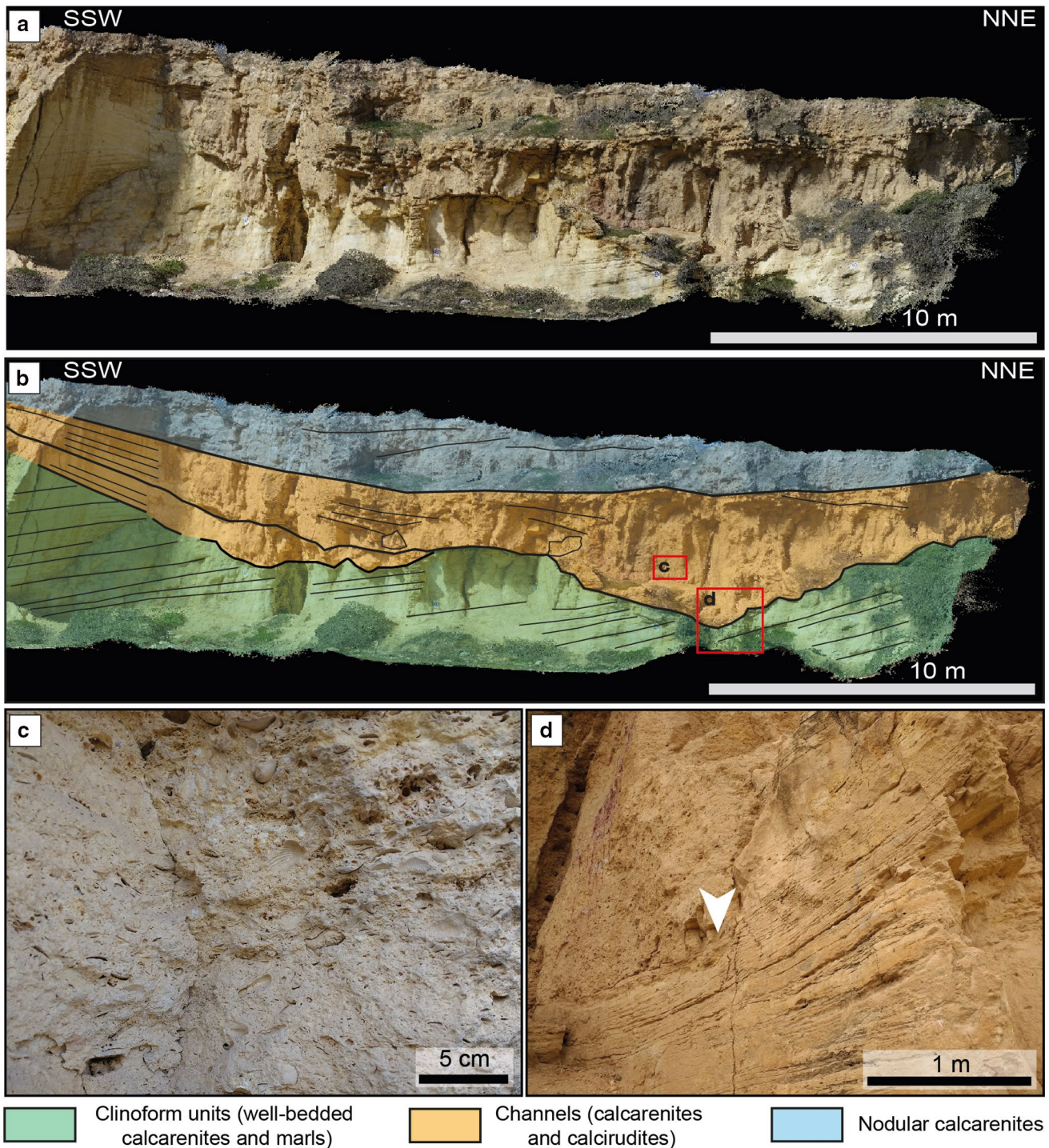
Fig. 7 Details on Location 2—Beer Sheva Quarry. **a** Close-up view of the photogrammetric model at the northern part of the outcrop and **b** interpretation of the canyon fill. **c** Field photograph of the channel fill consisting of a bioclastic calcirudite and **d** close-up of the wall of the quarry with observable clinoform units truncated by the erosional base of the channel (white arrow) and its calciruditic fill

canyon, (2) sediment delivered to the canyon by gravity processes, and (3) in-situ canyon flank accumulation.

Erosional processes and products

The seismic profiles show that the canyon flanks were steeper during the first stages of canyon incision (Oligocene–Early Miocene, Druckman et al. 1995) and progressively became
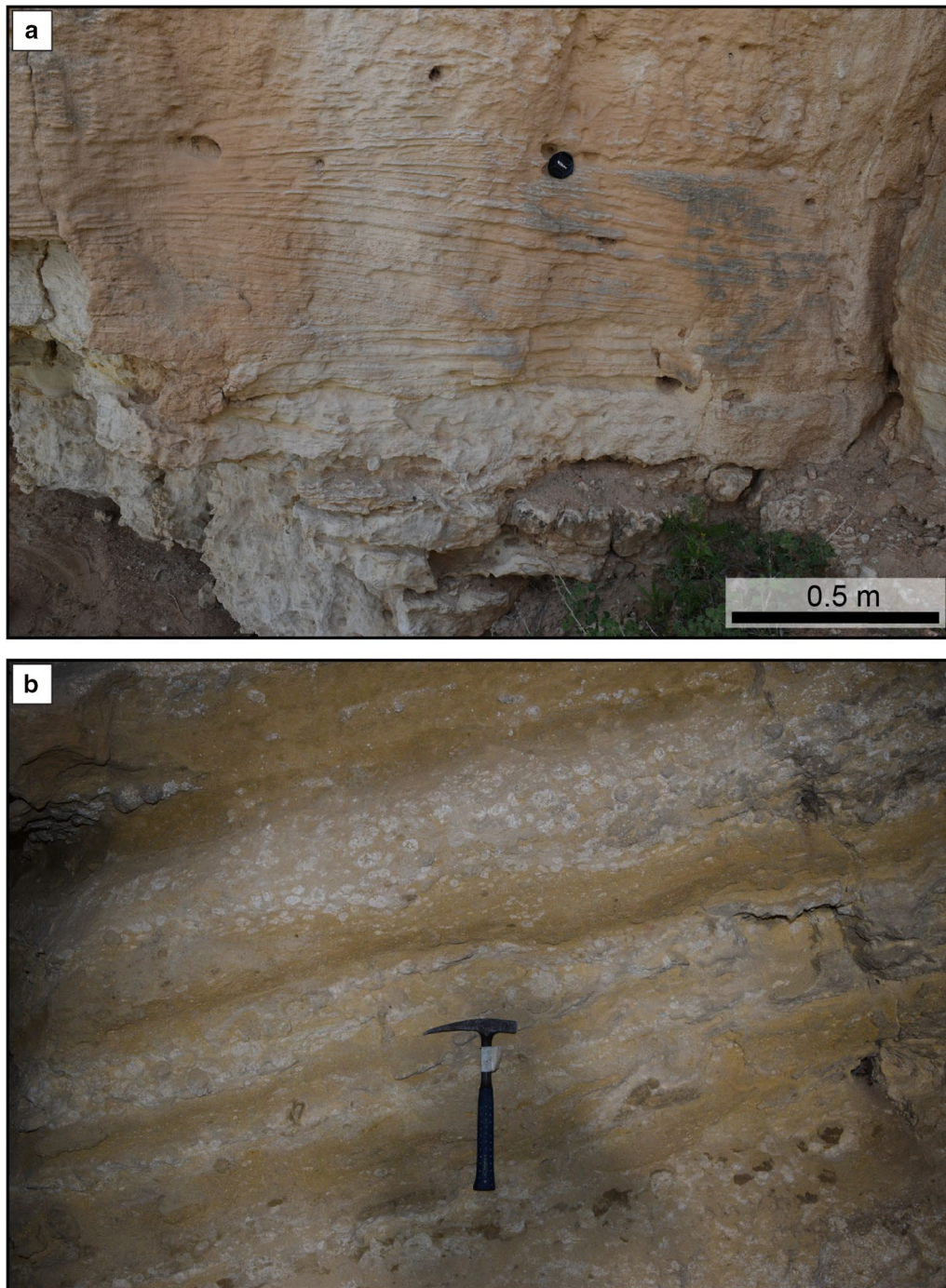
Fig. 8 Field photographs of **a** cross-bedded calcarenites at Location 3 and **b** rhodolith-pavement beds at Location 4—Ofakim Park

gentler, especially at the northeastern margin (Figs. 3, 4). This latter morphology has been interpreted by Druckman et al. (1995) as a submarine landslide scar that contributed to the headward erosion of the canyon and its subsequent incision into the shelf edge. Based on the canyon trace of Buchbinder and Zilberman (1997) for the Upper Miocene (Fig. 1), Location 1 would be located on the canyon edge at

relatively shallow-water depths. Here, the canyon incision is represented by an erosional unconformity marked by a basal breccia over the chalk and marl of the Eocene Avedat Group (Fig. 5a, d). This poorly sorted breccia is rich in basement-derived clasts, which suggest short transport and a local sediment source. The breccia could have been emplaced by mass-transport processes (e.g., rockfalls and debris
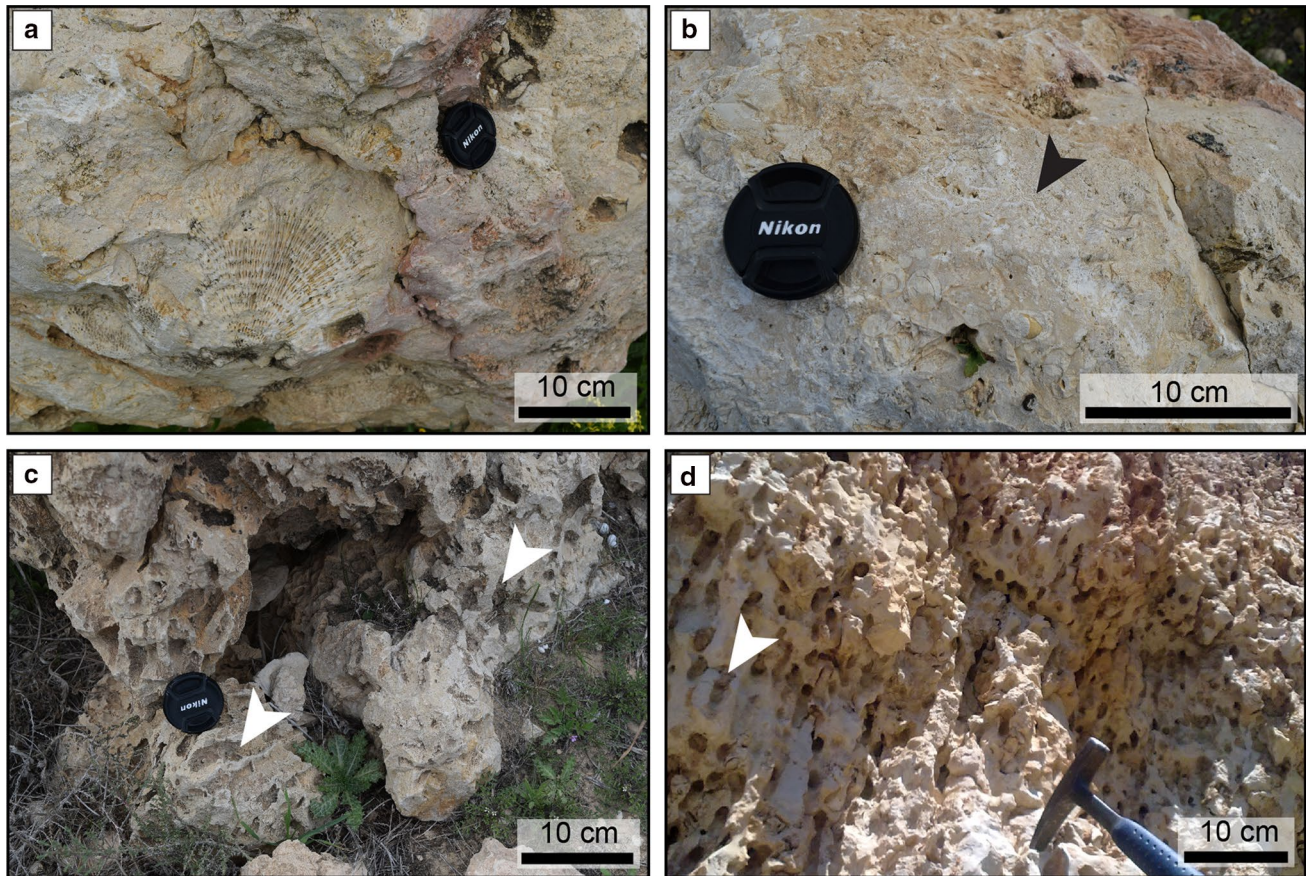
Fig. 9 Corals of Location 4—Ofakim Park. **a** Example of coral, *Tarbellastrea*, embedded in a thick stromatolitic crust. **b** Close-up of the stromatolitic crust with abundant borings of *Lithophaga* sp. Black arrow indicates microbial lamination. **c** Molds of *Porites* tube (white arrows) surrounded by a thick stromatolitic crust, as in the Messinian *Porites* reefs from the Sorbas Basin in Spain (**d**)

avalanches) originated in the steep canyon margins during canyon incision. Similar erosional unconformities associated with basal conglomerate/breccia deposits and interpreted as slope failure products have also been described in other submarine canyons (Morris and Busby Spera 1988; Cronin and Kidd 1998; Di Celma et al. 2014; Maier et al. 2018; Janocko and Basilici 2021).

Sediment delivery by gravity-driven processes

At the seismic scale, the canyon fill comprises the Miocene deposits of the Bet Eshel Formation, the Pattish Formation and younger units (white colour in Figs. 2, 3, and 4). These deposits are represented by low to moderate amplitude reflections which mimic the morphology of the canyon axial part and become chaotic towards the steep flanks of the canyon (Figs. 3, 4). Such features are also observable at the outcrop scale at Location 1. There, calcarenites reworked from the platform adjacent to the canyon were deposited in clinobeds mimicking the morphology of the erosional canyon base (Fig. 5e). Some of these clinobeds are slightly slumped (Fig. 5f), probably representing the small-scale equivalent of the chaotic reflections found toward the canyon incision (Figs. 3, 4). Mass-transport deposits, including slumps, are reported as a common phenomenon in the sediments deposited along canyon flanks (Cronin et al. 2005; He et al. 2014; Mulder et al. 2019; Su et al. 2020; Janocko and Basilici 2021), including the continental margin of Israel (Druckman et al. 1995; Frey Martinez et al. 2005).

The coarse-grained calcarenite clinoforms, composed of a local mixture of siliciclastics and lithoclasts from the platform through which the canyon was incised, are probably the products of erosion near the canyon border. Apart from the early lithified material, these include reworked bioclastic sediments containing organisms living on the platform, mostly bivalves and gastropods (Fig. 6c). Together with the molluscs, echinoids and bryozoans they are the main components in the clinoform facies. The original carbonate factory from which bioclasts were derived is not observed at any of the study outcrops, very likely due to the substantial regional erosion during the MSC or a ravinement process during the Pliocene reflooding

(Buchbinder and Zilberman 1997). However, the bioclastic components can be observed as parautochthonous to allochthonous accumulations formed by downslope sediment flows (Fig. 6c, d). In the case of the proximal Location 1, the canyon slope is covered by submarine colluvium, which was derived from close-by sources, as is evident by the well-preserved components.

The calcarenite clinobeds have a uniform thickness, but local thinning of the beds is recognizable from the flanks towards the canyon axis (Figs. 6, 7). Instabilities at the canyon margins likely promoted rockfalls, debris falls and slumps of the sediment on the canyon flanks and triggered sediment gravity flows (Fig. 10a; Khripounoff et al. 2012). The transport capacity of these flows decayed down

the canyon flanks, as shown by the grain-size gradation observed along the clinobeds (Adams et al. 2004; Playton et al. 2010), i.e., from coarser grains in the proximal part of the clinobeds to finer grained calcisiltites towards the canyon axis at Location 2.

The channels that locally truncate the uppermost part of the clinoforms at Location 2 (Figs. 6, 7) are cut-and-fill structures interpreted as the result of sustained high-energy sediment gravity flows. These flows probably originated in the adjacent platform and were funnelled into the depressed areas in correspondence to the canyon incision, resulting in erosion and channel development as described in similar carbonate systems (Braga et al. 2001; Vigorito et al. 2005; Puga-Bernabéu et al. 2008). The evolution of the channel
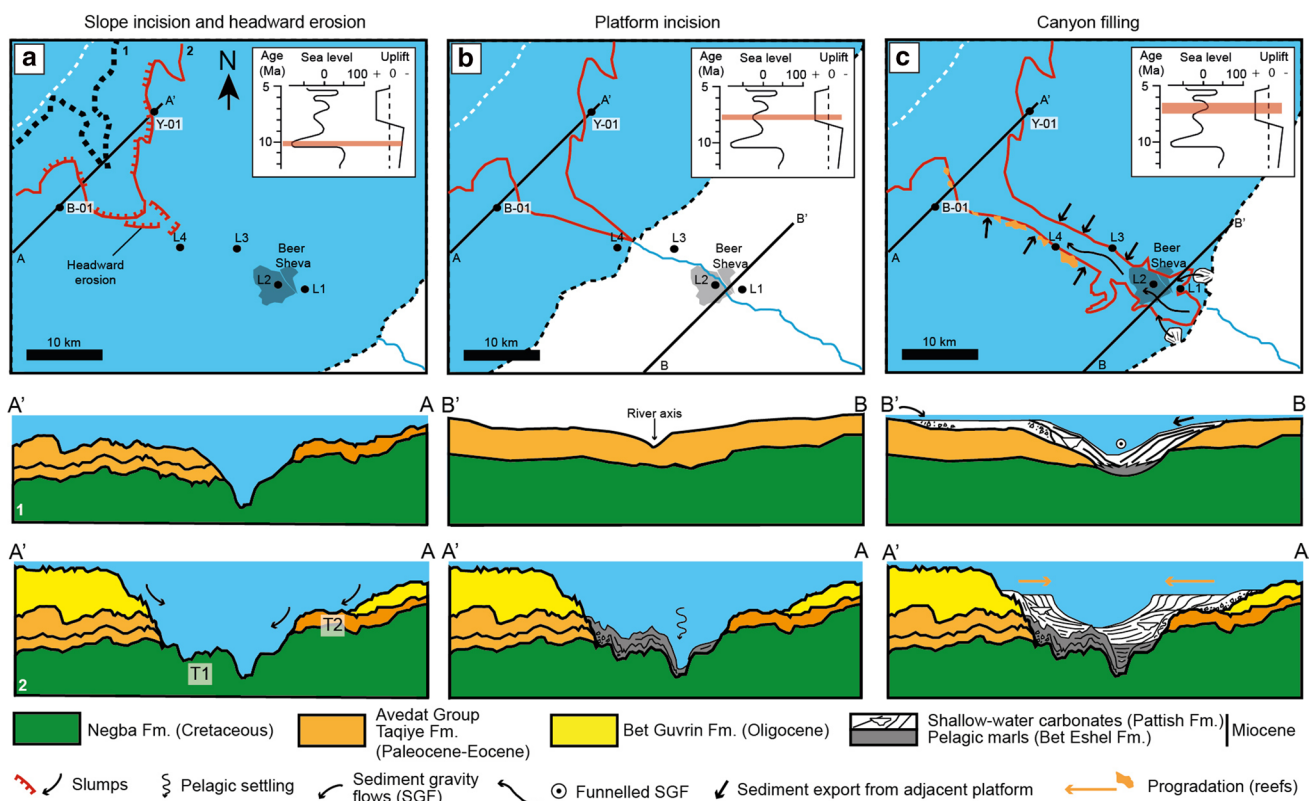

Fig. 10 Model showing the Oligocene–Miocene evolution of the Beer Sheva Canyon based on the age model of Buchbinder et al. (1993). **a** Inferred palaeogeography of the Beer Sheva Canyon during the Oligocene (1) and Middle Miocene (2) incision phases. White dashed line represents the present-day coastline. Black dashed line represents the Middle Miocene coastline. Cross sections of the Beer Sheva canyon during the Oligocene (1, thick pointed line) and Middle Miocene (2, red line) are shown in the lower part of the figure. The trace of the Oligocene Beer Sheva Canyon is based on the isopach map of Druckman et al. (1995). The inset with the sea-level and uplift curves is based on Buchbinder and Zilberman (1997). **b** Inferred palaeogeography of the Beer Sheva Canyon during the Early Upper Miocene incision phase. Proximal (B–B') and distal (A–A') cross sections are shown in the lower part of the figure. Note that the Beer Sheva Canyon incision into the platform (red line) likely ended with fluvial cap-

ture (see Discussion in text). Pelagic marls of the Bet Eshel formation started to be deposited at the centre of the canyon. **c** Inferred palaeogeography of the Beer Sheva Canyon during the Upper Miocene canyon filling phase. Outline of the Beer Sheva Canyon (red line) modified from Buchbinder and Zilberman (1997). Proximal (B–B') and distal (A–A') cross sections are shown in the lower part of the figure. The instability and collapse of the canyon margins producing rockfalls and sediment gravity flows that originate from the Pattish Formation and the facies succession observed at Location 2. Some of the sediment gravity flows were funneled and resulted in the channels documented in Figs. 6, 7. The carbonate production at the margins was enhanced and rhodolith beds and later coral–stromatolite reefs developed. The slopes associated to these reefs display a progradational pattern towards the canyon interior as observed in the seismic profiles (Fig. 4)

fills comprises three facies from bottom to top: (1) accumulation of cm-size clasts of early consolidated calcarenites at the base; (2) massive calcirudite; and (3) poorly laminated calcarenites. Such a facies succession indicates a gradual decrease in energy of the sediment gravity flows through these channels in line with the progressive channel filling (Fig. 7b). The presence of coral debris in the channelized facies is consistent with a shallow-water platform source for these sediment flows.

The alternations of mass-transport deposits with periods of sedimentation in quiet-water conditions allowed the bioturbating organisms to occupy and bioturbate the distal facies. Therefore, the intensely bioturbated tops of the clinobeds are likely related to breaks in sedimentation, which may be attributed to the episodic nature of the gravity flows or lower rates of sediment supply (Reolid et al. 2019).

At Location 3, the decimetric well-sorted medium-to-fine-grained cross-bedded calcarenites are interpreted as megaripples and small dunes on the canyon floor and/or lateral bars based on their position close to the canyon margin (Fig. 1). Thick sub-horizontal beds interbedded with the cross beds were likely the result of the turbidity currents that originated in the upper canyon and then flowed along the canyon axis.

Carbonate sediment produced at the canyon flanks

The gently inclined clinoforms with abundant rhodoliths at Location 4 are the first evidence of facies with little transport from the factory area (Fig. 8b). Rhodoliths are commonly interpreted as occurring in oligophotic environments, such as those during the Middle Miocene, when they formed spectacular accumulations along the Mediterranean margins (Braga et al. 2009, 2010; Benisek et al. 2012; Brandano and Ronca 2014). Most of the rhodolith beds in the Mediterranean Sea occur from 9 to 150 m water depth, with most of them forming within depths of 30–75 m (Basso et al. 2017). Speeds of at least 80 cm/s are needed to initiate the movement of rhodoliths around 5 cm in size, such as those observed at Location 4 (Harris et al. 1996) and, therefore, are interpreted as autochthonous to parautochthonous slope deposits (Benisek et al. 2012). However, the main evidence of in-situ carbonate production at the canyon flanks occurs, where the flanks display sigmoidal reflections on top of terrace 2, locally with sharp edges, prograding towards the canyon interior (Fig. 4d). This reflection geometry is characteristic of clinoform units associated with rimmed carbonate platforms, as reported from the Great Bahama Bank (Eberli and Ginsburg 1989) or the Maldives (Betzler et al. 2016; Reolid et al. 2020), but also in onshore outcrops (Riding et al. 1991; Pomar 1991). These clinoform units are likely related to the development of fringing reefs and associated slope deposits at the margins of the Beer

Sheva Canyon. Extensive shelf-edge reef barriers rim the steep heads of shelf-incised canyons in the Great Barrier Reef (Puga-Bernabéu et al. 2011, 2013). Fringing reefs are also known to develop on the margins of steep slopes on modern isolated carbonate platforms (Eberli and Ginsburg 1989; Reolid et al. 2017a, 2020; Ling et al. 2021) and in a few hinterland-attached margins, such as the Red Sea (Katz et al. 2015; Torfstein et al. 2020). In the case of the Red Sea, the dominant conditions are oligotrophic and arid, but perpetuated by strong episodic pluvial input events (Katz et al. 2015; Torfstein et al. 2020). The conditions on the margins of the Beer Sheva Canyon were probably similar to those.

The sharp edges of some clinoforms observed in the seismic profiles are probably the equivalent of the reefs observed at Location 4, and they can also be interpreted as small fringing reefs attached to the flanks of the canyon (Fig. 10c). The reef framework with abundant *Porites* skeletons covered by thin coralline algal–foraminiferal crusts overgrown by thick stromatolitic crusts (Fig. 9a–c) is similar to those described from the Late Miocene in western Mediterranean outcrops (Riding et al. 1991; Braga and Martín 1996; Reolid et al. 2014, 2017b; Fig. 9d) and also in the central/eastern Mediterranean in Greece (Brachert et al. 2006). Coral reefs were first described in the Beer Sheva area by Buchbinder et al. (1993). Such *Porites*–stromatolite reefs were traditionally described as ''aberrant'' representing the progressive restricted water-circulation in the Mediterranean as a prelude of the Messinian Salinity Crisis (Esteban 1979). However, the presence of thick microbial deposits has been proved to be common in Holocene reefs of normal-marine conditions, such as the barrier reef of Tahiti (Camoin et al. 1999), the Great Barrier Reef (Braga et al. 2019), and the Great Bahama Bank (Reolid et al. 2017a).

Canyon evolution and controls

Classic models of sequence stratigraphy have postulated that submarine canyons are active during sea-level lowstands when shelves are exposed and rivers are able to erode them (Posamentier and Vail 1988; Vail et al. 1991). In contrast, with rising sea level and highstands, submarine canyons are detached from the sediment source area and sediment supply diminishes. However, such a response of canyons to sea-level fluctuations is not universal and several authors have suggested that local factors, such as shelf and slope morphology, subsidence and sediment supply, may be more significant than sea-level changes (Galloway et al. 1991; McHugh et al. 2002; Gamberi 2020).

Buchbinder et al. (1993) recognized that the overall onshore distribution of the Neogene sediments in the area of Beer Sheva shows incomplete correlation with Haq's et al. (1987) global coastal–onlap curve. Buchbinder et al. (1993) proposed a strong tectonic overprint (uplift) associated with

the convergence of the Arabian and the Eurasian plate, which produced the westward tilt and uplift of the shelf and overprinted the eustatic trend. This uplift occurred during the early Middle Miocene, before the deposition of the Pattish Formation (Buchbinder et al. 1993; Fig. 2).

The first evidence of erosion linked to the formation of the Beer Sheva Canyon is recorded in the Oligocene Bet Guvrin Formation, and the incision affected down to Upper Cretaceous strata (Negba Formation, Figs. 3, 4). This is consistent with previous models that place the canyon incision in the Early Oligocene (Buchbinder et al. 1993; Druckman et al. 1995), although some authors date the start of canyon incision to the Oligocene–Miocene transition or directly in the Early Miocene (Bar et al. 2013). In any case, the main incision phase leading to the excavation of the Beer Sheva Canyon ended before the start of the deposition of the Pattish Formation during the Tortonian (Druckman et al. 1995). The age constraint for this area is not robust enough for detailed reconstructions of canyon evolution, but according to the data presented in this study and previous literature, it is possible to distinguish three main stages of canyon development: (1) slope incision and headward erosion, (2) platform incision and (3) canyon filling (Fig. 10).

The first incision phase corresponds to the submarine canyon inception and its excavation in the slope of a steep submarine escarpment during the Early Oligocene (Fig. 10a) (Buchbinder et al. 1993; Druckman et al. 1995). This phase is recognizable in the seismic profiles by the deepest V-shaped incision (Figs. 3, 4, 10a). Erosion and bypass characterise this phase that show no to little deposition. The U-shape of the canyon cross section observed in the seismic profiles, with relatively steep margins and the subhorizontal terraces T1 and T2 (Fig. 10a), reflects an important incision phase that led to the widening of the canyon. This incision must have taken place after deposition of the Bet Guvrin Formation (Oligocene–earliest Miocene) (Fig. 10a). Druckman et al. (1995) interpreted a large slope failure during the latest Middle Miocene was responsible for the canyon widening. Such an event led to the upslope canyon head retrogression and progressive headward erosion in a similar fashion to the classic model of Farre et al (1983) for siliciclastic canyons, which has also been interpreted in carbonate canyon systems (Puga-Bernabéu et al. 2011; Tournadour et al. 2017). Headward erosion eventually led the canyon to be incised into the shelf during the Late Miocene (Druckman et al. 1995). At the regional scale, the moderate eustatic fall at the beginning of cycle TB3.2 during the Late Tortonian (Haq et al. 1987) was coincident with an important tectonic uplift (Buchbinder and Zilberman 1997). The resultant sea-level fall is interpreted to have led to the incision of fluvial systems, one of which could have captured and connected with the Beer Sheva Canyon

head (Fig. 10b). This interpretation is consistent with the uniform rectilinear morphology of the canyon trace in plain view, which extends inland > 20 km from the location of the slumped area (Fig. 10a, b). Progressive sea-level rise and relative tectonic quiescence during the latest Tortonian and earliest Messinian re-flooded the area adjacent to the Beer Sheva Canyon resulting in the deposition of the early canyon fill within the previous river valley, which is recorded by the Bet Eshel Formation (Fig. 10c). At this stage, a carbonate factory dominated by molluscs, echinoids and bryozoans (Buchbinder and Zilberman 1997) developed on the platform adjacent to the Beer Sheva Canyon. This carbonate factory was still responding to the rearrangement of the Mediterranean's oceanographic setting in the aftermath of the loss of connection to the Indian Ocean and global cooling (Bialik et al. 2022; Cornacchia et al. 2021). The sediment on the platform was prone to reworking by storms and longshore currents and was likely pirated by the canyon, as is observed in channels cross-cutting modern and ancient carbonate platforms (Eberli and Ginsburg 1989; Puga-Bernabéu et al. 2008; Betzler et al. 2013; Reolid et al. 2017a). Axial incision and related margin collapses (Baztan et al., 2005) caused by sediment gravity flows generated along the canyon margins and funnelled through the canyon axis contributed to the enlargement of the canyon valley (e.g., breccia deposits linked to slope failures; Fig. 5). Locally and at shallow-water proximal canyon settings, the relative abundance of siliciclastic grains in the canyon fill suggests a nearby source of terrigenous sediment (Fig. 10c), Before and during the redeposition of shallow-water materials, the canyon axis and distal canyon areas were dominated by hemipelagic settling that resulted in the formation of the marls of the Bet Eshel Formation (Figs. 3, 4, 10c) (Druckman et al. 1995).

The late canyon filling phase is recorded by the sediments of the Pattish Formation that overlie part of the Bet Eshel Formation (Buchbinder et al. 1993; Buchbinder and Zilberman 1997; Fig. 2). This phase was dominated by sediment-gravity flows and mass transport that formed the clinoform units and channels observed at Location 2 (Fig. 10c). Storm and longshore currents continued delivering sediment from the 'factory area' on the platform to the canyon margins. The sediment at the steep canyon margins was also susceptible to instabilities that led to slumps and sediment gravity flows (Figs. 5, 6). These processes not only resulted in the deposition of the calcarenite clinobeds, but they also could have generated downslope-eroding sediment flows (Gaudin et al. 2006; Laberg et al. 2007; Puga-Bernabéu et al. 2008; Arzola et al. 2008), being channelized into the canyon (i.e., the channels crosscutting the clinoform units at Location 2, Figs. 6, 7). This process is observed in modern canyons, where canyon heads collect sediment provided by longshore and/or storm currents (Lewis and Pantin 2002; Puig et al. 2004; Normark et al. 2006; Gamberi et al. 2017). The latest canyon fill was

locally supplied by fringing coral reefs developed close to the canyon rims (Buchbinder et al. 1993; Buchbinder and Zilberman 1997; Fig. 10c). Buchbinder et al. (1993) attributed the *Porites* reefs to in-situ carbonate production at the canyon margins during the sea-level highstand that predates the third-order cycle 3.3 from Haq et al.'s (1987) curve. This sea-level highstand, approximately between 6.05 and 5.90 Ma when extrapolated to Miller et al.'s (2011) curve, is approximately coincident with the last progradation stages of the *Porites* reefs in the Sorbas Basin in the westernmost part of the Mediterranean (Sánchez-Almazo et al. 2007; Reolid et al. 2016). In the Sorbas Basin, the last progradation stages of reef occurred during a relative sea-level highstand and ended with an abrupt sea-level fall that produced a regional erosion surface and the occurrence of onlapping evaporites (Riding et al. 1991; Martín and Braga 1994; Sánchez-Almazo et al. 2007; Reolid et al. 2016). In the case of the Beer Sheva Canyon, such an erosion surface is not visible because of the outcrop nature, but Buchbinder et al. (1993) described the occurrence of Upper Miocene evaporites in cores that overlie the clinoform units associated with the reefs of the Pattish Formation. The last depositional unit at Location 2, the nodular calcarenites with abundant vertical trace fossils (mostly *Thalassinoides*), is interpreted as the most advanced stage of the canyon evolution. The homogeneity of the facies, completely bioturbated and lacking any sedimentary structure, likely represented the progressive fill of the accommodation space in the proximal parts of the canyon. These are the last carbonates deposited in the canyon and predate the Plio–Pleistocene deposits and the migration of the coastline to its present-day position (Buchbinder and Zilberman 1997; Fig. 2).

Conclusions

Carbonate deposits (Pattish Formation) developed along the margins of the pre-evaporitic Messinian Beer Sheva Canyon in Israel were investigated and analysed in four outcrops and complemented with the interpretation of seismic profiles, from which, the following conclusions are drawn:

The canyon has three main seismic facies of fill (1) Subparallel reflections that mimic the morphology of the canyon; (2) chaotic reflections that overlie the subparallel ones, and (3) sigmoidal reflections, locally with sharp edges at the canyon margins. The first seismic facies is equivalent to the pelagic marls of the Bet Eshel Formation. The other two seismic facies are equivalent to the bioclastic calcarenite clinobeds with slump and channels and to the coral–stromatolite reefs and reef slopes of the Pattish Formation, respectively. At the canyon margins, there is also a 4-m-thick breccia unit that

separates the Pattish Formation from the eroded basement and that cannot be detected at the seismic-scale resolution.

According to the geometry and composition of the canyon fill, it is possible to distinguish three main stages of canyon development:

(1) slope incision and headward erosion: the first incision phase consisted of erosion and bypassing due to tectonic uplift and eustatic fall during the Early Oligocene, followed by a second incision phase linked to a large slope failure during the latest Middle Miocene.
(2) platform incision: the canyon incised the shelf and connected with a fluvial system in the Late Miocene, during a period of eustatic sea-level fall coincident with regional tectonic uplift.
(3) canyon filling: subsequent reflooding of the platform led to the development of a shallow-water carbonate factory that supplied sediment to the canyon.

Filling geometries and facies depend on the dominant sedimentary processes in each phase. Sediment gravity flows, generated by slumps (canyon flank failures) or by littoral drift and storm currents, were the most frequent transport mechanisms down-canyon and formed the bioclastic calcarenite clinobeds. Locally, sustained sediment gravity flows were funnelled and became confined forming channels that eroded the clinobeds. The facies within the channels consists of calcirudite with large centimetric lithoclasts. In contrast, the coral–stromatolite reefs and their prograding reef slopes were mostly the result of enhanced carbonate production at the canyon margins with minor occurrence of sediment gravity flows.

The submarine canyon phase ended with the deposition of evaporites during the Messinian Salinity Crisis. Later the canyon was filled up by Pliocene–Pleistocene deposits.

References

Adams EW, Schroder S, Grotzinger JP, McCormick DS (2004) Digital reconstruction and stratigraphic evolution of a microbial-dominated, isolated carbonate platform (terminal proterozoic, Nama Group, Namibia). J Sediment Res 74:479–497. https://doi.org/10.1306/122903740479

Agisoft (2021) Agisoft metashape

Arzola RG, Wynn RB, Lastras G, Masson DG, Weaver PPE (2008) Sedimentary features and processes in the Nazaré and Setúbal submarine canyons, west Iberian margin. Mar Geol 250:64–88. https://doi.org/10.1016/j.margeo.2007.12.006

Avni Y, Segev A, Ginat H (2012) Oligocene regional denudation of the northern Afar dome: Pre- and syn-breakup stages of the Afro-Arabian plate. Bull Geol Soc Am 124:1871–1897. https://doi.org/10.1130/B30634.1

Bar O, Gvirtzman Z, Feinstein S, Zilberman E (2013) Accelerated subsidence and sedimentation in the Levant basin during the late tertiary and concurrent uplift of the Arabian platform: tectonic versus counteracting sedimentary loading effects. Tectonics 32:334–350. https://doi.org/10.1002/tect.20026

Bar O, Zilberman E, Feinstein S, Calvo R, Gvirtzman Z (2016) The uplift history of the Arabian plateau as inferred from geomorphologic analysis of its northwestern edge. Tectonophysics 671:9–23. https://doi.org/10.1016/j.tecto.2016.01.004

Basso D, Babbini L, Ramos-Esplá AA, Salomidi M (2017) Mediterranean rhodolith beds. In: Riosmena-Rodríguez R, Nelson W, Aguirre J (eds) Rhodolith/Maërl beds: a global perspective. Coastal research library, vol 15. Springer, Cham

Baztan J, Berneé S, Olivet JL, Rabineau M, Gaudin DM, Réhault JP, Canals M (2005) Axial incision: the key to understand submarine canyon evolution (in the western Gulf of Lion). Mar Petrol Geol 22:805–826

Benisek M-F, Marcano G, Betzler C, Mutti M (2012) Facies and stratigraphic architecture of a miocene warm-temperate to tropical fault-block carbonate platform, sardinia (Central Mediterranean Sea). Carbonate systems during the oligocene-miocene climatic transition. Wiley-Blackwell, Oxford, UK, pp 129–148

Betzler C, Eberli GP, Kroon D, Wright JD, Swart PK, Nath BN, Alvarez-Zarkikian CA, Alonso-Garcia M, Bialik OM, Blatter CL, Guo JA, Haffen S, Horozal S, Inoue M, Jovane L, Lanci L, Laya JC, Mee AL, Lüdmann T, Nakakuni M, Niino K, Petruny LM, Pratiwi SD, Reijmer JJG, Reolid J, Slagle AL, Sloss CR, Su X, Yao Z, Young JR (2016) The abrupt onset of the modern South Asian monsoon winds. Sci Rep 6:29838. https://doi.org/10.1038/srep29838

Brachert TC, Reuter M, Kroeger KF, Lough JM (2006) Coral growth bands: a new and easy to use paleothermometer in paleoenvironment analysis and paleoceanography (late Miocene, Greece). Paleoceanography. https://doi.org/10.1029/2006PA001288

Braga JC, Martín JM (1996) Geometries of reef advance in response to relative sea-level changes in a Messinian (uppermost Miocene) fringing reef (Cariatiz reef, Sorbas Basin, SE Spain). Sediment Geol 107:61–81. https://doi.org/10.1016/S0037-0738(96)00019-X

Braga JC, Martin JM, Wood JL (2001) Submarine lobes and feeder channels of redeposited, temperate carbonate and mixed siliciclastic-carbonate platform deposits (Vera Basin, Almeria, southern Spain). Sedimentology 48:99–116. https://doi.org/10.1046/j.1365-3091.2001.00353.x

Braga JC, Vescogni A, Bosellini FR, Aguirre J (2009) Coralline algae (Corallinales, Rhodophyta) in western and central mediterranean messinian reefs. Palaeogeogr Palaeoclimatol Palaeoecol 275:113–128. https://doi.org/10.1016/j.palaeo.2009.02.022

Braga JC, Martín JM, Aguirre J, Baird CD, Grunnaleite I, Jensem NB, Puga-Bernabéu Á, Sælen G, Talbot MR (2010) Middle-Miocene (Serravallian) temperate carbonates in a seaway connecting the Atlantic Ocean and the Mediterranean Sea (North Betic Strait, S Spain). Sediment Geol 225:19–33. https://doi.org/10.1016/j.sedgeo.2010.01.003

Braga JC, Puga-Bernabéu Á, Heindel K, Patterson MA, Birgel D, Peckmann J, Sánchez-Almazo IM, Webster JM, Yokoyama Y, Riding R (2019) Microbialites in last glacial maximum and deglacial reefs of the Great Barrier Reef (IODP Expedition 325, NE Australia). Palaeogeogr Palaeoclimatol Palaeoecol 514:1–17. https://doi.org/10.1016/j.palaeo.2018.10.007

Brandano M, Ronca S (2014) Depositional processes of the mixed carbonate–siliciclastic rhodolith beds of the Miocene Saint-Florent Basin, northern Corsica. Facies 60:73–90. https://doi.org/10.1007/s10347-013-0367-z

Buchbinder B (1996) Middle and Upper Miocene reefs and carbonate platforms in Israel. In: Franseen EK, Esteban M, Ward WC, Rouchy JM (eds) Models for carbonate stratigraphy from miocene reef complexes of mediterranean regions. SEPM concepts in sedimentology and paleontology vol 5, pp 333–345

Buchbinder B, Zilberman E (1997) Sequence stratigraphy of Miocene-Pliocene carbonate-siliciclastic shelf deposits in the eastern Mediterranean margin (Israel): effects of eustasy and tectonics. Sediment Geol 112:7–32. https://doi.org/10.1016/S0037-0738(97)00034-1

Buchbinder B, Martinotti GM, Siman-Tov R, Zilberman E (1993) Temporal and spatial relationships in Miocene reef carbonates in Israel. Palaeogeogr Palaeoclimatol Palaeoecol 101:97–116. https://doi.org/10.1016/0031-0182(93)90154-B

Camoin GF, Gautret P, Montaggioni LF, Cabioch G (1999) Nature and environmental significance of microbialites in Quaternary reefs: the Tahiti paradox. Sediment Geol 126:271–304. https://doi.org/10.1016/S0037-0738(99)00045-7

CloudCompare (2021) CloudCompare (version 2.11.3). 3D point cloud and mesh processing software. Open Source Project

Coletti G, Basso D, Betzler C, Robertson AHF, Bosio G, El Kateb A, Foubert A, Meilijson A, Spezzaferri S (2019) Environmental evolution and geological significance of the Miocene carbonates of the Eratosthenes Seamount (ODP Leg 160). Palaeogeogr Palaeoclimatol Palaeoecol 530:217–235. https://doi.org/10.1016/j.palaeo.2019.05.009

Cornacchia I, Brandano M, Agostini S (2021) Miocene paleoceanographic evolution of the Mediterranean area and carbonate production changes: a review. Earth Sci Rev 221:103785. https://doi.org/10.1016/j.earscirev.2021.103785

Cronin BT, Kidd RB (1998) Heterogeneity and lithotype distribution in ancient deep-sea canyons: point Lobos deep-sea canyon as a reservoir analogue. Sediment Geol 115:315–349. https://doi.org/10.1016/S0037-0738(97)00099-7

Cronin BT, Akhmetzhanov AM, Mazzini A et al (2005) Morphology, evolution and fill: implications for sand and mud distribution in filling deep-water canyons and slope channel complexes. Sediment Geol 179:71–97. https://doi.org/10.1016/j.sedgeo.2005.04.013

Dabrio CJ, Esteban M (1981) The Coral Reef of Nijar, Messinian (Uppermost Miocene), Almeria Province, S E Spain. SEPM J Sediment Res 51:521–539. https://doi.org/10.1306/212F7CCA-2B24-11D7-8648000102C1865D

Di Celma C, Teloni R, Rustichelli A (2014) Large-scale stratigraphic architecture and sequence analysis of an early Pleistocene submarine canyon fill, Monte Ascensione succession (Peri-Adriatic basin, eastern central Italy). Int J Earth Sci 103:843–875. https://doi.org/10.1007/s00531-013-0984-3

Druckman Y, Buchbinder B, Martinotti GM, Siman Tov R, Aharon P (1995) The buried Afiq Canyon (eastern Mediterranean, Israel): a case study of a tertiary submarine canyon exposed in late Messinian times. Mar Geol 123:167–185. https://doi.org/10.1016/0025-3227(94)00127-7

Eberli GP, Ginsburg RN (1989) Cenozoic progradation of northwestern Great Bahama Bank, a record of lateral platform growth and sea-level fluctuations. In: Crevello PD, Wilson JL, Sarg JF, Read JF (eds) Carbonate platform and basin development. SEPM Spec Publ 44, Tulsa, Oklahoma, pp 339–351

Esteban M (1979) Significance of the upper miocene coral reefs of the Western Mediterranean. Palaeogeogr Palaeoclimatol Palaeoecol 29:169–188. https://doi.org/10.1016/0031-0182(79)90080-4

Exon N, Hill P, Mitchell C, Post A (2005) Nature and origin of the submarine Albany canyons off southwest Australia. Aust J Earth Sci 52:101–115. https://doi.org/10.1080/08120090500100036

Farre JA, McGregor BA, Ryan WBF, Robb JM (1983) Breaching the shelfbreak passage from youthful to mature phase in submarine canyon evolution. SEPM Spec Publ 33:25–39

Fleischer L, Varshavsky A (2002) A lithogtratigraphic data base of oil and gas wells drilled in Israel. Jerusalem

Frey Martinez J, Cartwright J, Hall B (2005) 3D seismic interpretation of slump complexes: examples from the continental margin of Israel. Basin Res 17:83–108. https://doi.org/10.1111/j.1365-2117.2005.00255.x

Galloway WE, Dingus WF, Paige R (1991) Seismic and depositional facies of Paleocene-Eocene Wilcox Group Submarine canyon fills, Northwest Gulf Coast, USA. In: Link MH, Weimer P (eds) Seismic facies and sedimentary processes of submarine fans and turbidite systems. Springer-Verlag, New York, pp 247–271

Gamberi F (2020) Systems supplying sediment to canyon heads (SSSCHs) in the Tyrrhenian Sea: the past and the present as a key to understanding deep-sea stratigraphy. Mar Pet Geol 119:104470

Gamberi F, Rovere M, Marani MP, Dykstra M (2015) Modern submarine canyon feeder-system and deep-sea fan growth in a tectonically active margin (northern Sicily). Geosphere 11:307–319. https://doi.org/10.1130/GES01030.1

Gamberi F, Breda A, Mellere D (2017) Depositional canyon heads at the edge of narrow and tectonically steepened continental shelves: comparing geomorphic elements, processes and facies in modern and outcrop examples. Mar Pet Geol 87:157–170

Gardosh M, Weimer P, Flexer A (2011) The sequence stratigraphy of mesozoic successions in the Levant margin, southwestern Israel: a model for the evolution of southern Tethys margins. Am Assoc Pet Geol Bull 95:1763–1793. https://doi.org/10.1306/02081109135

Gaudin M, Mulder T, Cirac P et al (2006) Past and present sedimentary activity in the Capbreton Canyon, southern Bay of Biscay. Geo-Mar Lett 26:331–345. https://doi.org/10.1007/s00367-006-0043-1

Gvirtzman G, Buchbinder B (1969) Outcrops of neogene formations in the central and southern coastal plain, Hashephela and Beer Sheva regions, Israel. Israel Geol Surv Bull 50

Haq BU, Hardebbol J, Vail PR (1987) Chronology of fluctuating sea levels since the triassic. Science (80) 235:1156–1167. https://doi.org/10.1126/science.235.4793.1156

Harris PT, Tsuji Y, Marshall JF, Davies PJ, Honda N, Matsuda H (1996) Sand and rhodolith-gravel entrainment on the mid- to outer-shelf under a western boundary current: Fraser Island continental shelf, eastern Australia. Mar Geol 129:313–330. https://doi.org/10.1016/0025-3227(96)83350-0

He Y, Zhong G, Wang L, Kuang Z (2014) Characteristics and occurrence of submarine canyon-associated landslides in the middle of the northern continental slope, South China Sea. Mar Pet Geol 57:546–560

Hirsch F (2005) The oligocene-pliocene of Israel. In: Hall JK, Krasheninnikov VA, Hirsch F, Benjamini C, Flexer A (eds) Geological framework of the levant, vol II. The Levantine Basin and Israel. Historical Productions-Hall, Jerusalem, pp 459–488

Janocko J, Basilici G (2021) Architecture of coarse-grained gravity flow deposits in a structurally confined submarine canyon (late Eocene Tokaren Conglomerate, Slovakia). Sediment Geol 417:105880. https://doi.org/10.1016/j.sedgeo.2021.105880

Katz T, Ginat H, Eyal G, Steiner Z, Braun Y, Shalev S, Goodman-Tchernov BN (2015) Desert flash floods form hyperpycnal flows in the coral-rich Gulf of Aqaba, Red Sea. Earth Planet Sci Lett 417:87–98. https://doi.org/10.1016/j.epsl.2015.02.025

Khripounoff A, Crassous P, Lo Bue N, Dannielou B, Silva Jacinto R (2012) Different types of sediment gravity flows detected in the Var submarine canyon (northwestern Mediterranean Sea). Prog Oceanogr 106:138–153. https://doi.org/10.1016/j.pocean.2012.09.001

Klaucke I, Masson DG, Kenyon NH, Gardner JV (2004) Sedimentary processes of the lower Monterey Fan channel and channel-mouth lobe. Mar Geol 206:181–198. https://doi.org/10.1016/j.margeo.2004.02.006

Laberg JS, Guidard S, Mienert J, Vorren TO, Haflidason H, Nyg A (2007) Morphology and morphogenesis of a high-latitude canyon; the Andøya Canyon, Norwegian Sea. Mar Geol 246:68–85. https://doi.org/10.1016/j.margeo.2007.01.009

Lewis KB, Pantin HM (2002) Channel-axis, overbank and drift sediment waves in the southern Hikurangi Trough, New Zealand. Mar Geol 192:123–151. https://doi.org/10.1016/S0025-3227(02)00552-2

Ling A, Eberli GP, Swart PK, Reolid J, Stainbank S, Rüggeberg A, Betzler C (2021) Middle Miocene platform drowning in the Maldives associated with monsoon-related intensification of currents. Palaeogeogr Palaeoclimatol Palaeoecol 567:110275. https://doi.org/10.1016/j.palaeo.2021.110275

Maier KL, Johnson SY, Hart P (2018) Controls on submarine canyon head evolution: Monterey Canyon, offshore central California. Mar Geol 404:24–40. https://doi.org/10.1016/j.margeo.2018.06.014

Maier KL, Paull CK, Caress DW, Anderson K, Nieminski NM, Lundsten E, Erwin BE, Gwiazda R, Fildani A (2020) Submarine-fan development revealed by integrated high-resolution datasets from La Jolla Fan, offshore California, U.S.A. J Sediment Res 90:468–479. https://doi.org/10.2110/jsr.2020.22

Martín J, Braga JC (1994) Messinian events in the Sorbas Basin in southeastern Spain and their implications in the recent history of the Mediterranean. Sediment Geol 90:257–268. https://doi.org/10.1016/0037-0738(94)90042-6

Martín JM, Braga JC, Betzler C (2001) The Messinian Guadalhorce corridor: the last northern, Atlantic-Mediterranean gateway. Terra Nova 13:418–424

Martín JM, Braga JC, Aguirre J, Puga-Bernabéu Á (2009) History and evolution of the North-Betic Strait (Prebetic Zone, Betic Cordillera): a narrow, early Tortonian, tidal-dominated, Atlantic-Mediterranean marine passage. Sediment Geol 216:80–90

Martín JM, Braga JC, Sánchez-Almazo IM, Aguirre J (2010) Temperate and tropical carbonate-sedimentation episodes in the Neogene Betic basins (southern Spain) linked to climatic oscillations and changes in Atlantic-Mediterranean connections: constraints from isotopic data. In: Mutti M, Piller W, Betzler C (eds) Carbonate systems during the Oligocene-Miocene climatic transition. IAS Spec Publ 42, pp 49–70

Martinotti GM, Siman-Tov R, Rosenfeld A (1981) Notes on the stratigraphy of the Saqiye Group as determined from foraminifera. Geological survey of Israel report P/3/81, Jerusalem

McHugh CMG, Damuth JE, Mountain GS (2002) Cenozoic mass-transport facies and their correlation with relative sea-level change, New Jersey continental margin. Mar Geol 184:295–334. https://doi.org/10.1016/S0025-3227(01)00240-7

Miller K, Mountain G, Wright J, Browning J (2011) A 180-million-year record of sea level and ice volume variations from continental margin and deep-sea isotopic records. Oceanography 24:40–53. https://doi.org/10.5670/oceanog.2011.26

Mitchell JK, Holdgate GR, Wallace MW, Gallagher SJ (2007) Marine geology of the Quaternary Bass Canyon system, southeast Australia: a cool-water carbonate system. Mar Geol 237:71–96. https://doi.org/10.1016/j.margeo.2006.10.037

Morris WR, Busby Spera CJ (1988) Sedimentologic evolution of a submarine canyon in a forearc basin, upper cretaceous rosario formation, San Carlos, Mexico. Am Assoc Pet Geol Bull 72:717–737. https://doi.org/10.1306/703C8F0B-1707-11D7-8645000102C1865D

Mulder T, Gillet H, Hanquiez V, Reijmer JJG, Droxler AW, Recouvreur A, Fabregas N, Cavilhes T, Fauquenberge K, Blank DG, Guiastrennec L, Seibert C, Bashah S, Bujan S, Ducassou E, Principaud M, Conesa G, Le Gof J, Ragusa J, Busson J, Borgomano J (2019) Into the deep: A coarse-grained carbonate turbidite valley and canyon in ultra-deep carbonate setting. Mar Geol 407:316–333. https://doi.org/10.1016/j.margeo.2018.11.003

Mutti E, Normark WR (1987) Comparing examples of modern and ancient turbidite systems; problems and concepts. In: Legget JK, Zuffa GG (eds) Marine clastic sedimentology: concepts and case studies. Graham and Trotman, London, UK, pp 1–38

Neev D (1960) A pre-Neogene erosion channel in the southern coastal plain of Israel. Israel Geol Surv Bull 25

Normark WR, Piper DJW, Sliter R (2006) Sea-level and tectonic control of middle to late Pleistocene turbidite systems in Santa Monica Basin, offshore California. Sedimentology 53:867–897. https://doi.org/10.1111/j.1365-3091.2006.00797.x

Papadimitriou N, Deschamps R, Symeou V, Souque C, Gorini C, Nader FH, Blanpied C (2018) The tectonostratigraphic evolution of Cenozoic basins of the Northern Tethys: the northern margin of the Levant Basin. Oil Gas Sci Technol 73:77. https://doi.org/10.2516/ogst/2018085

Playton TE, Janson X, Kerans C (2010) Carbonate slopes. In: James NP, Dalrymple RW (eds) Facies models 4. GEOtext 6: Geological Association of Canada, St John's, Newfoundland, pp 449–476

Pomar L (1991) Reef geometries, erosion surfaces and high-frequency sea-level changes, upper Miocene Reef Complex, Mallorca, Spain. Sedimentology 38:243–269. https://doi.org/10.1111/j.1365-3091.1991.tb01259.x

Posamentier HW, Vail PR (1988) Eustatic controls on clastic deposition II—sequence and systems tract models. In: Wilgus CK, Hastings BS, Kendall CGSC, Posamentier HW, Ross Ca, Van Wagoner JC (eds) Sea-level changes: an integrated approach. SEPM Spec Publ 42, pp 125–154

Puga-Bernabéu Á, Martín JM, Braga JC (2008) Sedimentary processes in a submarine canyon excavated into a temperate-carbonate ramp (Granada Basin, southern Spain). Sedimentology 55:1449–1466. https://doi.org/10.1111/j.1365-3091.2008.00952.x

Puga-Bernabéu Á, Webster JM, Beaman RJ, Guilbaud V (2011) Morphology and controls on the evolution of a mixed carbonate–siliciclastic submarine canyon system, Great Barrier Reef margin, north-eastern Australia. Mar Geol 289:100–116. https://doi.org/10.1016/j.margeo.2011.09.013

Puga-Bernabéu Á, Webster JM, Beaman RJ, Guilbaud V (2013) Variation in canyon morphology on the Great Barrier Reef margin, north-eastern Australia: the influence of slope and barrier reefs. Geomorphology 191:35–50. https://doi.org/10.1016/j.geomorph.2013.03.001

Puga-Bernabéu Á, Webster JM, Beaman RJ, Reimer PJ, Renema W (2014) Filling the gap: a 60 ky record of mixed carbonate-siliciclastic turbidite deposition from the Great Barrier Reef. Mar Pet Geol 50:40–50. https://doi.org/10.1016/j.marpetgeo.2013.11.009

Puig P, Ogston AS, Mullenbach BL, Nittourer CA, Parsons JD, Stemberg RW (2004) Storm-induced sediment gravity flows at the head of the Eel submarine canyon, northern California margin. J Geophys Res Ocean. https://doi.org/10.1029/2003JC001918

Reolid J, Betzler C, Braga JC, Martín JM, Lindhorst S, Reijmer JJG (2014) Reef slope geometries and facies distribution: controlling factors (Messinian, SE Spain). Facies 60:737–753. https://doi.org/10.1007/s10347-014-0406-4

Reolid J, Betzler C, Braga JC (2016) Amplitude of late Miocene sea-level fluctuations from karst development in reef-slope deposits (SE Spain). Sediment Geol 345:145–153. https://doi.org/10.1016/j.sedgeo.2016.09.009

Reolid J, Betzler C, Eberli GP, Grammer GM (2017a) The importance of microbial binding in neogene-quaternary steep slopes. J Sediment Res 87:567–577. https://doi.org/10.2110/jsr.2017.28

Reolid J, Betzler C, Singler V, Stange C, Lindhorst S (2017b) Facies variability in mixed carbonate–siliciclastic platform slopes (Miocene). Facies 63:11. https://doi.org/10.1007/s10347-016-0489-1

Reolid J, Betzler C, Lüdmann T (2019) The record of Oligocene-Middle Miocene paleoenvironmental changes in a carbonate platform (IODP Exp. 359, Maldives, Indian Ocean). Mar Geol 412:199–216. https://doi.org/10.1016/j.margeo.2019.03.011

Reolid J, Betzler C, Braga JC, Lüdmann T, Ling A, Eberli GP (2020) Facies and geometry of drowning steps in a Miocene carbonate platform (Maldives). Palaeogeogr Palaeoclimatol Palaeoecol 538:109455. https://doi.org/10.1016/j.palaeo.2019.109455

Riding R, Martín JM, Braga JC (1991) Coral-stromatolite reef framework, Upper Miocene, Almeria, Spain. Sedimentology 38:799–818. https://doi.org/10.1111/j.1365-3091.1991.tb01873.x

Sánchez-Almazo IM, Braga JC, Dinarès-Turell J, Martin JM, Spiro B (2007) Palaeoceanographic controls on reef deposition: the Messinian Cariatiz reef (Sorbas Basin, Almería, SE Spain). Sedimentology 54:637–660. https://doi.org/10.1111/j.1365-3091.2006.00853.x

Steinberg J, Gvirtzman Z, Gvirtzman H, Ben-Gai Y (2008) Late tertiary faulting along the coastal plain of Israel. Tectonics 27:1–22. https://doi.org/10.1029/2007TC002151

Su M, Lin Z, Wang C, Kuang Z, Liang J, Chen H, Liu S, Zhang B, Luo K, Huang S, Wu Q (2020) Geomorphologic and infilling characteristics of the slope-confined submarine canyons in the Pearl River Mouth Basin, northern South China Sea. Mar Geol 424:106166. https://doi.org/10.1016/j.margeo.2020.106166

Talling PJ (2014) On the triggers, resulting flow types and frequencies of subaqueous sediment density flows in different settings. Mar Geol 352:155–182. https://doi.org/10.1016/j.margeo.2014.02.006

Torfstein A, Kienast SS, Yarden B, Rivlin A, Isaaacs S, Shaked Y (2020) Bulk and export production fluxes in the Gulf of Aqaba, Northern Red Sea. ACS Earth Sp Chem 4:1461–1479. https://doi.org/10.1021/acsearthspacechem.0c00079

Tournadour E, Mulder T, Borgomano J, Gillet H, Chabaud L, Ducassou E, Hanquiez V, Etinne S (2017) Submarine canyon morphologies and evolution in modern carbonate settings: the northern slope of Little Bahama Bank, Bahamas. Mar Geol 391:76–97. https://doi.org/10.1016/j.margeo.2017.07.014

Vail PRF, Audemard SAPR, Bowman D, Eisner N, Perecruz C (1991) The stratigraphic signatures of tectonics, eustacy and sedimentology-an overview. In: Einsele G, Ricken W, Seilacher A (eds) Cycles and events in stratigraphy. Springer-Verlag, Berlin, pp 618–659

Vigorito M, Murru M, Simone L (2005) Anatomy of a submarine channel system and related fan in a foramol/rhodalgal carbonate sedimentary setting: a case history from the Miocene syn-rift Sardinia Basin, Italy. Sediment Geol 174:1–30. https://doi.org/10.1016/j.sedgeo.2004.10.003

Zilberman E (2018) The geological map of Israel, 1:50,000. Sheet 14-IV, Be'er Sheva. Jerusalem